August 2020

Fabrication and Application of Flexible Sensors

Tallis Huther da Costa
Louisiana State University and Agricultural and Mechanical College

FABRICATION AND APPLICATION OF FLEXIBLE SENSORS

A Dissertation

Submitted to the Graduate Faculty of the
Louisiana State University and
Agricultural and Mechanical College
in partial fulfillment of the
requirements for the degree of
Doctor of Philosophy

in

The School of Electrical Engineering and Computer Science

by
Tallis Huther da Costa
B.E., Pontifical Catholic University of Rio Grande do Sul, 2013
December 2020

ACKNOWLEDGMENTS

I am indebted to many friends and colleagues that, in one way or another, helped me through the course of my research. First, I am grateful for my advisor Dr. Jin-Woo Choi, who early taught me the importance of doing science the right way, following logical steps, and not losing focus of the big picture. But most importantly, preserving integrity as engineers and scientists should do.

I would like to thank the committee members Dr. Anne Grove, Dr. Todd Monroe, Dr. Kidong Park, and Dr. Jian Xu, for their valuable time and suggestions. Also, I want to extend my gratitude to professor Dr. Hsiao-Chun Wu, Young-Ho Shin, Dr. Aquiles Parodi, Jong-Yoon Park, Beth Cochran, Dr. Edward Song, Ryan Tortorich, Pedro Chacon Dominguez, Dr. Hamed Shamkhalichenar, and Limeng Pu.

TABLE OF CONTENTS

ABSTRACT

A transfer printing method was developed to transfer carbon nanotubes (CNTs) from polyethylene terephthalate (PET) film to poly(dimethyl siloxane) (PDMS) polymer. Carbon nanotubes are composed of carbon atoms arranged in a honeycomb lattice structure, which are electrically conducting. When embedded in a nonconducting polymer, carbon nanotubes impart electrical conductivity to the nanocomposite, thus forming a nanocomposite that has potential applications in highly sensitive strain and pressure sensors. Several printing methods have been studied to deposit carbon nanotubes onto PDMS, including inkjet printing. Inkjet printing is a desirable deposition method since it is low-cost, simple, and allows the processing of aqueous-based inks. However, directly inkjet printing carbon nanotubes onto PDMS has been a challenge because the printed film becomes non-uniform due to the uneven drying of the droplets. Therefore, a method of transfer printing was developed to embed carbon nanotubes uniformly in PDMS.

The transfer printing method consists of first inkjet printing patterns of carbon nanotubes onto a PET film, which quickly absorbs the aqueous ink and allows uniformity of the printed carbon nanotube patterns. The next step is spin-coating PDMS on the PET film to cover the carbon nanotube patterns, followed by curing the PDMS. The following step is thermally treating the PET film to promote the transfer of carbon nanotubes to PDMS, and finally peeling off PDMS from PET film to complete the transfer of carbon nanotube patterns. The transferred patterns had widths as small as 125 µm, while the obtained PDMS thickness was as low as 27.1 µm, which enabled the fabrication of highly sensitive force and pressure sensors.

The transfer printing method was employed to fabricate a two-dimensional force sensor, which was composed of lines of carbon nanotubes in the x and y directions. The transduction

mechanism lies in the generation of strain on the carbon nanotube pattern. When strain is produced, the resistance of the pattern changes due to the increase or decrease of the number of conduction paths in the carbon nanotube pattern. The practical application as a two-dimensional sensor was shown by monitoring the touch force exerted by multiple objects on the sensor.

Due to the flexibility and stretchability of PDMS, fabricated air pressure sensors were capable of detecting small pressure differences. The sensors were composed of a circular diaphragm containing inkjet-printed carbon nanotube patterns. When air pressure increased on one side of the diaphragm, the deflection caused a strain on the CNT line, thus changing its resistance. Pressure sensors with a diaphragm diameter of five millimeters, diaphragm thickness of 27.1 μm showed sensitivity of 10.99 percent change in resistance per kilopascal (%/kPa) and limit of detection of 3.1 Pa. The pressure sensor has potential applications in monitoring minute air pressure differences such as those generated by the breathing pattern. The application of the highly sensitive and biocompatible pressure sensor was shown through the measurement of the pressure generated by a 3D-printed respiratory system.

CHAPTER 1. INTRODUCTION

1.1. Motivation

The development of flexible sensors has dramatically been benefited from novel fabrication methods in recent years. A critical step in the fabrication of flexible sensors is the deposition of nanomaterials that bring functionality to the sensor. For example, depositing electrically conductive nanomaterials onto polymers produces a conductive nanocomposite which has the characteristic of changing the resistance when a given stimulus is applied, such as strain. One of the methods employed to deposit nanomaterials is inkjet printing, which is a simple and cost-effective method for printing aqueous-based inks. However, the direct inkjet printing of aqueous-based inks onto polymers such as poly(dimethyl siloxane) (PDMS) creates patterns that are non-uniform due to the irregular wetting and evaporation of droplets. Therefore, the main focus of this work is the development of a transfer printing method that produces electrically conductive and uniformly distributed carbon nanotubes on the polymer PDMS.

Several deposition methods have been developed to print nanomaterials onto substrates. For example, in spray coating, a nanomaterial dispersion is directly sprayed on the substrate to form large area and low resistivity conducting films. However, functional devices require patterned conductive areas, such that additional patterning steps increase the complexity of spray coating. Along with patterning ability, the requirements for deposition methods include simplicity and cost-effectiveness. Inkjet printing is a method of deposition of nanomaterials that is both simple and cost-effective, allowing patterning of the nanomaterial while printing. Additionally, it is especially suited to print aqueous dispersions of nanomaterials. Therefore, by employing inkjet printing of carbon nanotubes to fabricate conductive films onto PDMS, it is possible to achieve a simple and cost-effective transfer printing method for the fabrication of force and pressure sensors.

Flexible sensors are especially suited for the measurement of signals related to the human body, such as strain, pressure, and touch sensors. In the fabrication of flexible sensors, polymers are used as the structural element because of their flexibility, stretchability, and biocompatibility. The main advantage is their low elastic modulus, compared to plastics or silicon (Table 1). The low modulus allows a much higher response to the stimulus, that is, polymers deform more than rigid materials, and this effect translates into higher sensitivity of the sensor. Another advantage is the processability of polymers through simple mixing of base monomers with a curing agent and subsequent polymerization. By depositing carbon nanotubes, it is possible to make conductive nanocomposites in which carbon nanotubes are supported by the polymer matrix, allowing high strains to be achieved. Besides, PDMS is biocompatible, allowing its use in diverse applications such as wearable sensors, cell culturing in microchannels, and many others.

Table 1. Comparison of mechanical properties of selected materials used in MEMS/flexible sensors.

Material	**Elastic Modulus**	**Poisson's Ratio**	**Ref.**
Polycrystalline silicon	165 GPa	0.22	[1]
Polymide (Kapton® Type 100 HN Film)	3.2 GPa	0.34	[2]
Parylene-C	2.76 PGa	0.4	[3]
PDMS (Sylgard 184)	1.32–2.97 MPa[1]	0.49	[4]

PDMS: poly(dimethyl siloxane)
[1]Curing temperature range: 25 °C to 200 °C.

1.2. Objectives

The main objective is to develop the technique composed of inkjet printing carbon nanotube patterns onto polyethylene terephthalate (PET) film and subsequently transferring those patterns to PDMS. Particular issues that were addressed are the improvement of the variability of the process and the ability to peel off thin films (~30 μm) of PDMS from PET. By using this method, a range of sensors was fabricated and characterized, such as force sensors and pressure sensors. Moreover, the sensors can be used in applications such as breathing monitors and flexible biochemical sensors. Specific objectives of this work are presented in the next subsections.

1.2.1. Preparation of Inkjet Printing

To realize the inkjet printing of carbon nanotubes, the cartridge needs to be adapted to receive a carbon nanotube ink. Here a commercial cartridge is adapted to receive a carbon nanotube ink. The commercial office inkjet printer contains a cartridge with a high number of nozzles (one hundred and twenty nozzles) that is best suited for printing large areas of carbon nanotubes. On the other hand, cartridges designed for point-of-sale printing only contain a small number of nozzles (eight nozzles), which can be individually controlled. By individually controlling the nozzles and the cartridge position, patterns with improved resolution can be achieved. Therefore, both approaches can be employed to print carbon nanotubes onto flexible substrates. Many physical factors play a role while printing, such as the propensity of the ink to drip after inserted into the cartridge, optimization of the printing resolution, printing speed vs. coalition of droplets, etc. Such factors are characterized and optimized for the printing of conductive patterns of carbon nanotubes.

1.2.2. Transfer Printing of CNT Patterns

Inkjet printing is used to define micrometer-resolution patterns onto PET film. The next step is to transfer those patterns to PDMS. By using this method, the difficulties of printing directly to

PDMS are overcome, such as the coalescence of droplets, the coffee ring effect, and the non-uniform printing. Compared to other methods in the literature, this method is simpler, allows control of the quantity of CNTs deposited and control of the pattern resolution. Specifically, improvement of the sheet resistance of the patterns on PDMS and reduction of the variability are important issues to be addressed.

1.2.3. Fabrication of Sensors with the Transfer Printing Technique

The transfer printing technique described here allows patterning of carbon nanotubes on PDMS to be realized. Since direct inkjet printing of aqueous inks on PDMS generates irregularities on the printed pattern, the ink is first printed onto PET film and then transferred to PDMS. With this technique, two-dimensional force sensors can be fabricated, air pressure sensors, humidity sensors, electrochemical sensors, etc.

The PDMS polymer offers low resistance to deformation induced by air pressure. This characteristic enables the fabrication of pressure sensors that detect lower than 10 Pa of differential pressure change. Also, by integrating lines of carbon nanotubes in a two-dimensional grid, it is possible to develop two-dimensional force sensors with greater sensitivity than those found in the literature.

1.3. Dissertation Outline

The chapters of this dissertation are organized in the following manner: Chapter 1 introduces the motivation of this work, the objectives, and the dissertation outline. Chapter 2 contains the literature review of composite elastomer for sensing applications and its fabrication methods. Chapter 3 develops the transfer printing of carbon nanotubes to PDMS. Chapter 4 presents the two-dimensional force sensing using the transfer printing technique. Chapter 5 presents the air pressure sensor fabricated using this technology. Chapter 6 presents a preliminary investigation of a sleep apnea sensor, and finally, Chapter 7 contains the conclusions and future work.

CHAPTER 2. LITERATURE REVIEW

2.1. Introduction

Flexibility is one of the requirements for wearable sensors, allowing the sensor to conform to body movements. The ability to stretch is of another importance for sensor-skin interaction. For example, the bending of fingers generates simultaneous flexure and stretching. Along with the choice of materials, patterning techniques affect the performance parameters of the sensors. For flexible sensors measuring pressure and motion, two approaches are used to achieve high sensitivity: (1) choosing a substrate with low Young's modulus such as polymer to provide higher deformations and (2) creating microstructures during fabrication which substantially improve the response of the sensor. The second approach includes microstructures such as pyramids [5], domes [6], and other rough surface morphologies [7], [8]. It is through a rational choice of materials and fabrication techniques that sensors can be tailored for a specific application.

The ability of a process to fabricate three-dimensional (3D) structures and form functional materials expands the list of available techniques beyond established silicon processes. Novel sensors require the integration of different functional materials such as structural elements, conductors, and biochemical components. Those materials are integrated in a variety of ways, including deposition, coating, assembly, printing, etc., which exemplifies the diversity of processes used in sensor fabrication.

Flexible sensors are especially suited for novel applications in healthcare, which are represented

---

This chapter was previously published as T. H. da Costa and J.-W. Choi, "Fabrication and Patterning Methods of Flexible Sensors Using Carbon Nanomaterials on Polymers," Advanced Intelligent Systems, vol. 2, art. 1900179, 2020. doi: 10.1002/aisy.201900179. Reprinted by permission of WILEY-VCH Verlag GmbH & Co. KGaA, Weinheim.

by non-invasive, measurement and real-time monitoring of biophysical [9] and biochemical [10], [11] signals from the human body, such as wrist pulse monitoring [12], strain measurement [13], humidity measurement [14], vibration detection [15], touch [16] and pressure [17] measurement, electrochemical detection [18], body temperature measurement [19], and many others. Many of the sensors can be applied for diagnosing diseases, monitoring a person's health, predicting cardiac events, and assisting in everyday tasks by providing signal feedback to actuators. Flexible sensors have promising applications in the next generation of healthcare technology.

2.2. Materials for Flexible Sensors

Mainly due to advances in semiconductor processing technologies, deposition and patterning of metals have achieved considerable progress in rigid substrates. However, functional sensors that employ large deformations present incompatibilities with surface-coated metal films. For example, microcracks and discontinuities are formed due to the difference in Young's modulus of metal and substrate. Besides, the high cost and complexity of semiconductor processes pose a challenge in developing novel flexible sensors. Research efforts have been directed to leverage the properties of nanomaterials while preserving the functionality and performance of the sensors, and the electrical conductivity of carbon nanomaterials make them especially useful in the development of conductors, active layers, and transduction elements in flexible sensors. Among the emerging types of carbon nanomaterials are carbon nanotubes, graphene and its derivatives, and carbon black. Carbon nanotubes (CNTs) are carbon atoms arranged in a cylindrical configuration where the diameter reaches up to 100 nm, and the length is of the order of micrometers [20]. Carbon nanotubes are excellent electrical conductors, with intrinsic conductivities up to 106 S/cm [21]. This property is employed in the fabrication of conductive films and electrodes. However, the conductivity of a printed CNT film significantly decreases from the intrinsic conductivity due to contact resistance, especially if the carbon nanotubes are not uniformly printed or form bundles [22]. A nanotube formed by a single layer of arranged carbon atoms is regarded as a single-walled carbon nanotube (SWCNT), while for multiple layers, it is regarded as a multi-walled carbon nanotube (MWCNT). The Young's modulus (E) of individual carbon nanotubes has been measured to be 1,054 GPa for SWCNT and 1,200 GPa for MWCNT [23]. Carbon nanotubes have been applied to a variety of sensors in microelectromechanical systems (MEMS) [24], chemical sensors [25], and many others [26]. Graphene is a single layer of carbon atoms that possesses outstanding mechanical, electrical, and chemical properties such as Young's modulus of 1.1 TPa, high carrier mobility [27], and rich chemistry [28]. Derivatives of graphene include graphene oxide (GO) and reduced graphene oxide (rGO), which are often preferred due to easier handling than pristine graphene and possessing more chemical interactions by attached functional groups. Due to the one-dimensional and two-dimensional nature of the described carbon nanomaterials, the majority of the carbon atoms are surface atoms, which are highly affected by conditions of the environment [29]. This property is used in chemical, gas, and humidity sensors where a higher surface area endows a higher sensitivity to the sensor.

Poly(dimethyl siloxane) (PDMS) is a versatile polymer material specially suited for flexible sensors since it has low Young's modulus and stretchability and can be easily processed by casting or spin coating. The use of PDMS in soft lithography has allowed a significant number of achievements, especially for the fabrication of microfluidic channels. For example, having a previously fabricated mold, PDMS can be cast and cured with the shape of the mold, thus replicating the features. PDMS can be itself a stamp, and features can be transferred to another substrate [30]. However, only structural assemblies are not enough to achieve functional physical and chemical sensors: it is necessary to deposit additional materials on PDMS to act as transduction elements. Therefore, the methods reviewed in the next section have been developed with the aim of printing and embedding carbon nanotubes in PDMS.

2.3. Processing of Carbon Nanomaterials for Flexible Sensors

Due to the electrical properties of carbon nanomaterials and the need to fabricate functional composites which are responsive to strain, several methods have been developed to embed carbon nanotubes in PDMS, such as in situ polymerization [31], mixing PDMS prepolymer and curing agent to CNT dispersion through solvents [32], mixing and grinding [33], screen printing [34], vacuum filtration [35], etc. In this section, each method is reviewed and analyzed with regard to its advantages and drawbacks. Table 2 summarizes material deposition methods on PDMS for the fabrication of flexible sensors.

Table 2. Methods for material deposition on PDMS.

Name of the method	**Short description**	**Materials**	**Sheet resistance/ resistivity**	**Ref.**
Vacuum filtration	Vacuum filtration followed by PDMS casting and peeling.	MWCNT on PDMS.	N.A.	[36]
Transfer printing	Transfer CVD-grown SWCNT from a silicon wafer to a flexible substrate such as PET.	SWCNT on PET, PDMS stamp	265 Ω/sq	[37]
Microcontact Printing	Vertically aligned MWCNT on PDMS.	Carbon nanotubes, PDMS	N.A.	[38]

(table cont'd.)

Name of the method	**Short description**	**Materials**	**Sheet resistance/ resistivity**	**Ref.**
Microcontact printing and cast molding	MWCNT and PDMS were separately dissolved in toluene and later mixed.	Carbon nanotubes, PDMS	16.6 Ω·cm	[39]
Spray coating	Spray coating SWCNT onto PDMS.	SWCNT, PDMS	328 Ω/sq	[40]
Direct mixing	Carbon black nanopowder was mixed in PDMS and cast onto a patterned glass mold. Carbon nanotubes were mixed with PDMS in a planetary mixer and cast onto an acrylic mold.	MWCNT on PDMS.	1 Ω·cm	[41], [42]
Indirect mixing	Graphite was microwave-exfoliated, dispersed into hexane, mixed with PDMS base, and then mixed with PDMS resin.	Exfoliated graphite on PDMS.	2.5 Ω·cm	[43]
Screen printing	Screen printing SWCNT on PDMS.	SWCNT, PDMS	100 Ω·cm	[34]
Inkjet printing	Inkjet-print aqueous solution of carbon nanotubes on PET film and transfer the material to PDMS after spin-coating PDMS.	Carbon nanotubes, PDMS	1.2 kΩ/sq	[44]

(table cont'd.)

Name of the method	Short description	Materials	Sheet resistance/ resistivity	Ref.
Electrophoretic deposition (EPD) and transfer micro molding	Carboxylated CNTs were dispersed in solution, and a gold-coated silicon was immersed and energized.	Carbon nanotubes, PDMS	N.A.	[45]
Drop-casting	Drop-casting carbon nanocoils on a polymer substrate and gold electrodes.	Carbon nanocoils, liquid crystal polymer	N.A.	[46]

N.A.: Not available

2.3.1. Filtration

Filtration of carbon nanomaterials can be employed for the formation of highly uniform films. A porous membrane is used to filtrate the carbon material, while positive or negative pressure is applied to control the flow of the solvent through the membrane. Carbon nanotubes that are dispersed in aqueous solution can be filtrated to produce a highly conductive film [47]. A potentially large area film can be fabricated (> cm^2) if the membrane is left in its pristine form. Alternatively, selective areas can be patterned on the membrane using photolithography, such that carbon nanotubes preferentially deposit on the patterned areas. Furthermore, the thickness of the film is controlled by the nanotube concentration and volume of ink used during filtration [48]. Transfer of the film to a receiving substrate is required, along with post-patterning of the film. Transfer of the film can be accomplished either by dissolving the membrane, directly pouring PDMS on the film with subsequent curing [36], [49], or using a PDMS stamp to transfer carbon nanotubes from the membrane to a final substrate [48]. Filtration has shown potential for large area, high conductivity patterns of carbon nanotubes, but the use of photolithography hinders low-cost fabrication of devices.

2.3.2. Transfer Printing Techniques

Transfer printing techniques comprise printing materials on a source substrate and transferring them with the use of a polymeric stamp. A molded stamp transfers only selected areas of the printed patterns, thereby serving as a patterning template. Alternatively, photolithography steps may be employed for patterning the required areas. The method can be used to pattern carbon nanotubes on a variety of substrates, such as polyethylene terephthalate (PET), poly(methyl methacrylate) (PMMA), glass, and silicon. It relies on the adhesion of carbon nanotubes to the surface of the receiving material. Materials with higher surface energy can receive carbon nanotubes just by contact [50]. Transfer printing is employed for transferring carbon nanotubes grown by chemical vapor deposition (CVD) on a silicon wafer (SiO_2/Si) to a flexible substrate. To this end, Cao *et al*. [37] transfer-printed single-walled carbon nanotubes from a silicon substrate to a PET film with the help of an elastomeric stamp of PDMS. Highly uniform SWCNT films were obtained with a low sheet resistance of 265 Ω/sq. Several photolithography steps were required to pattern SWCNT films onto the flexible substrate. In addition to transferring carbon nanotubes that are directly grown from CVD, transfer printing can be employed to transfer carbon nanotubes that are solution-processed. Hu *et al*. [51] filtrated single-walled carbon nanotubes and used a PDMS stamp to transfer the patterns to a PET film. They were able to achieve 50 μm of resolution using PDMS stamps and sheet resistance of 150 Ω/sq. In a modified transfer method by Lee *et al*. [52], a patterned film of SWCNT was embedded in

PDMS. First, a porous membrane of anodic aluminum oxide (AAO) was used to filtrate SWCNT. Then the membrane was dissolved in sodium hydroxide while the SWCNT film remained floating in the water. Subsequently, SWCNTs were transferred to a gold-coated silicon wafer by direct contact, and various patterns were defined with photolithography techniques. To embed SWCNTs in PDMS, the PDMS pre-polymer was poured onto the patterns, cured, and peeled off from the silicon substrate. Finally, the gold layer was etched away, exposing the SWCNT film. In this modified method, the patterned film of SWCNT embedded in PDMS was used as piezoresistors in the fabrication of pressure sensors.

Other methods of depositing solution-processed carbon nanotubes with subsequent transfer have been developed, such as streaming a CNT solution onto a substrate [53] and electrophoretic deposition of CNTs [45]. Meitl *et al*. [53] employed a method that consisted of streaming a solution of SWCNTs with sodium dodecyl sulfate (SDS) and another solution of methanol onto a rotating substrate. The methanol removes SDS from the solution, and the carbon nanotubes spread over the rotating substrate without agglomerating. A PDMS stamp was contacted afterward to transfer CNTs to a final substrate. Good uniformity was achieved on the first substrate. However, the films transferred to the final substrate presented poor uniformity. Moreover, the thickness of the film was not controllable. Xu *et al*. [45] obtained micropatterned CNTs on PDMS using electrophoretic deposition and subsequent transfer to PDMS. Carbon nanotubes were carboxylated in acid to improve water dispersibility. Silicon containing the desired microstructures and a gold seed layer were immersed into CNT solution and electrically energized. The negatively charged CNTs preferentially migrated and precipitated onto the gold seeds. The thickness of the CNT layer was determined by the duration of the experiment. PDMS was poured onto the sample and peeled off with CNTs attached to it. Although micropatterning was achieved, fabrication of the mold and deposition of the gold layer still required the use of standard lithographic methods, which would add cost and complexity. In addition, control over the deposition of CNTs was only achieved where gold was deposited.

Therefore, the transfer printing technique requires either pre- or post-photolithography steps to obtain patterned films of carbon nanotubes. In addition, due to the contact between the stamp and carbon nanotubes, only the surface nanotubes can be transferred, limiting control of the final thickness of the film.

2.3.3. Microcontact Printing

Microcontact printing (μCP) is a particular case of transfer printing. In microcontact printing, a PDMS stamp selectively contacts a composite ink and transfers the patterns to the desired substrate [54]. In contrast, transfer printing is the general term that applies for a variety of processes, having the characteristics of additive transfer, subtractive transfer, or deterministic assembly of materials [30]. Patterning carbon nanotube/PDMS composites in which the carbon nanotube film is embedded into PDMS has been developed through microcontact printing. Liu and Choi [39] mixed multi-walled carbon nanotubes (MWCNTs) with PDMS to form a composite ink, which was then spun on a silicon wafer. A micromachined PMMA stamp was used to selectively contact the ink and transfer the patterns to a final PDMS substrate. Curing and subsequent coating with a PDMS layer formed an all-elastomer strain sensor [39]. This method produced patterns of randomly oriented carbon nanotubes embedded in PDMS. To produce vertically aligned carbon nanotubes on PDMS, Kim *et al*. [38] used CVD to grow vertically aligned CNTs on a silicon wafer. With nanoimprint equipment, they transferred CNTs to a cured layer of PDMS by simply contacting the vertically aligned CNTs to the PDMS substrate. Although CNTs were successfully transferred, the height of CNTs shrunk from 400 μm to 60 μm due to the necessary pressure applied during contact. While their objective was to obtain vertically aligned CNTs, it was not possible to pattern CNTs with this method.

2.3.4. Spray Coating

Spray coating of carbon nanotube dispersions has been developed to form large area, low resistivity CNT films. A solution of dispersed nanomaterials is loaded into a spray gun and directly sprayed onto the receiving substrate. Both organic and aqueous solutions have been employed as the solvent, but due to the slow evaporation rate of aqueous solutions, non-uniform areas may occur. Moreover, the spray coating of multi-walled carbon nanotubes on PDMS obtained lower resistivity than graphene and reduced graphene oxide sprayed with similar conditions [55]. Lipomi *et al*. [40] directly sprayed an organic solution of SWCNTs onto PDMS, which was used to fabricate capacitive pressure sensors. Kim and Yun [56] patterned carbon nanotubes on PDMS with the assistance of spray coating and transfer printing. First, a photoresist layer was spun on a silicon substrate and selectively cured using photolithography methods. CNT was then sprayed on the photoresist layer. When the photoresist was developed, patterns of CNT remained on top of the exposed photoresist. A semi-cured PDMS layer was attached to the CNT film and then fully cured. Lastly, the PDMS layer was peeled off. This method provided sheet resistance of 96 Ω/sq for PDMS and 45 Ω/sq on photoresist when coated seven times, which was comparable to that of indium tin oxide (ITO) films (60-90 Ω/sq). Spray coating can be employed when the nanomaterials are in the form of an ink (organic or aqueous), it allows the formation of films with large area and low resistivity but relies heavily on photolithography for patterning the carbon nanomaterials, which adds complexity to the process.

2.3.5. Bulk Mixing

Mixing carbon nanotubes and PDMS has been performed directly and indirectly. In the direct method, a planetary centrifugal mixer was used to mix MWCNT with PDMS. A planetary centrifugal mixer rotates the viscous mixture in both directions, thus enabling mixing, deaeration, and dispersion simultaneously. Although no dispersion quality was provided, the MWCNT-PDMS composite with 7 wt% of MWCNT achieved a resistivity of ~1 Ω·cm [42]. The viscous composite was cast onto acrylic grooves formed by micro-milling and then partially cured. Then, another PDMS layer was cast on top of the MWCNT-PDMS composite, and the layers were fully cured. Finally, the cured PDMS having conductive tracks was peeled off from acrylic to form tactile sensors.

In the indirect method, carbon nanotubes and PDMS are separately dispersed in a common solvent and subsequently mixed into a uniform dispersion. The dispersion of carbon nanotubes in a suitable solvent entails the use of mild sonication to debundle agglomerated nanotubes. During and after mixing, the solvent is allowed to evaporate, leaving carbon nanotubes in the PDMS matrix. Through dispersion of MWCNT in different organic solvents for thirty minutes, it was found that after seventy hours, reaggregation of carbon nanotubes occurred in the order of toluene > chloroform > tetrahydrofuran (THF) > dimethylformamide (DMF). However, due to the incompatibility of THF and DMF with PDMS base, chloroform was best suited as the common solvent for carbon nanotubes and PDMS [57]. Noimark *et al*. [58] prepared a MWCNT-PDMS composite by mixing MWCNT in xylene, which is a solvent for both materials (MWCNT and PDMS). The dispersion was then mixed with PDMS to form a light-absorbing composite. The coatings were applied to the ends of optical fibers for the fabrication of ultrasound transmitters. Lee *et al*. [59] fabricated graphene and carbon nanotube nanocomposite strain sensors. MWCNT was added to the PDMS base, along with isopropyl alcohol (IPA) and Stoddard solvent, and sonicated for complete mixing. Crosslinker was then mixed, and the resulting nanocomposite was patterned onto a pure PDMS layer previously cured. The highest conductivity of the MWCNT-PDMS composite was 10^{-1} S/cm, with 12% of filler material. Bulk mixing therefore, can be employed when the filler has to be embedded into the base, creating a conductive polymer matrix instead of being patterned on the surface. Low resistivities can be achieved, but the compatibility and slow evaporation of the solvents are the main issue of this method.

2.3.6. Screen Printing

Screen printing has been developed to pattern carbon nanomaterials on flexible substrates. Differently from inkjet printing, the formulated paste contains a conductive carbon material which is mixed with binders and solvents. The highly viscous nature of the paste allows patterning with a stencil and subsequent evaporation of the solvent. Screen printing was used by Sekitani *et al*. [34] to coat SWCNT on PDMS. First, a SWCNT gel was formed by stirring SWCNT, ionic liquid, and 4-methly-2-pentanone for 16 h, followed by processing the gel in a jet-milling, which untangled or exfoliated the SWCNT. In the next step, 4-methly-2-pentanone and a fluorinated copolymer were added and stirred for another 16 h and dried in air for 6 h to produce a SWCNT paste. The paste was then screen-printed onto PDMS. A conductivity of 100 S/cm was achieved for SWCNT loading of 15.8 wt%.

The conductivity of carbon materials has been utilized in several applications ranging from flexible electronics, displays, sensors, supercapacitors, and batteries. Lowering the resistivity of carbon-based inks has been a challenge in these applications. Carbon materials diluted in water usually agglomerate, such that a dispersion agent is required. In conductive paste development, a binder is necessary, which increases the resistivity of the final paste. Recently, Phillips *et al*. [60] found that a mixture of graphite and carbon black (ratio of 6 to 1) produced optimal conductivity of 0.029 Ω·cm with good rheology properties for screen printing. The much smaller carbon black fills graphite gaps, resulting in a more conductive composite.

Liao *et al*. [61] reduced the resistivity further by adding dihydroxyphenyl-functionalized multi-walled carbon nanotubes (MWCNT-f-OH) to the carbon black and graphite mixture, along with using acrylic resin as a binder. The resistivity achieved was 29 Ω/sq when the mass fraction of the components was 10.2%, 3.0% and 4.1% for graphite, carbon black and MWCNT-f-OH, respectively. Screen printing is suitable for mass production of devices, achieving low resistivities, with a range of paste formulations available. However, the resolution of the features is relatively low (>75 μm) [62].

2.3.7. Inkjet Printing

Classically used for printing text and images, inkjet printing has recently found applications in many branches. Its advantages include the ability to print solutions of various materials, the extremely low waste and fine control of deposition parameters such as droplet location and number of printed droplets. Inkjet printing has been used to print thin-film transistors on plastic substrates [63], fabricate tactile sensors [64], two-dimensional force sensors [44], biosensors [65], and in a variety of other applications [66]. Inkjet printing can be classified into solution processing category which also includes spraying [53], [63], [64], aerosol-based [67], layer-by-layer [68], simple solution-evaporation [69], and dip coating [70], [71].

In one of the earliest developments in inkjet printing applied to flexible electronics, MWCNT carbon nanotubes were inkjet-printed onto transparency foil and paper [72]. In that study, carbon nanotubes were functionalized with nitric acid treatment so they could be dispersed in water. The achieved sheet resistivity was 40 kΩ/sq with multiple prints (minimum 30 prints to become conductive).

Kim *et al*. [73] inkjet-printed SWCNT directly onto PDMS substrate. The aqueous ink was developed with SWCNT and sodium dodecyl benzene sulfonate (SDBS), a surfactant that disperses nanomaterials in aqueous solutions. The ink was filtrated and inkjet-printed one to five times on previously cured PDMS. Treatment with water and nitric acid was performed to improve the sheet resistance. The minimum line width achieved was 80 µm, and the sheet resistance for five prints was 19.08 Ω/sq (with post-treatment). Cracks appeared on the CNT film upon stretching, which were attributed to the low adhesion of the PDMS surface to CNTs since the CNTs were not completely embedded into the PDMS matrix.

Ding *et al*. [74] used a dual method for achieving CNTs on PDMS. CNTs were vertically grown on a silicon wafer, followed by PDMS pouring and subsequent curing. Using inkjet printing, graphene oxide was deposited on top of the CNTs. The final step was to reduce the graphene oxide. By printing both materials, they achieved a sheet resistance of 386 Ω/sq.

Kumar *et al*. [75] inkjet-printed SWCNT modified with carboxylic groups on agarose gel and transferred the patterns to silicon oxide substrate by contact. Agarose gel is a porous hydrophilic polymer that readily absorbs water. The lowest sheet resistance achieved was 0.5 kΩ/sq for 40 prints.

Inkjet printing has been employed in the fabrication of flexible electrochemical and chemiresistive sensors. Due to the electrocatalytic activity of carbon nanotubes, electrodes composed uniquely of carbon nanotubes have been developed to measure analyte concentrations.

Furthermore, selectivity is attained by the addition of metal nanoparticles, which catalyze the reaction of specific analytes [76]. Tortorich *et al*. [77] inkjet-printed SWCNT on PET film, obtaining sheet resistance of 132 Ω/sq. The fabricated sensors were low cost, flexible and disposable, capable of measuring iron concentration through cyclic voltammetry. Da Costa *et al*. [78] inkjet-printed carbon nanotubes directly on paper for the fabrication of low cost and disposable dopamine sensors, while Song *et al*. [76] fabricated flexible chemiresistive sensors on PET film for glucose quantification. The carbon nanotubes were inkjet-printed as electrodes, and polyaniline nanowires were deposited between electrodes as resistive transduction elements.

Despite the versatility of inkjet printing, some drawbacks remain for inkjet printing of carbon nanotubes onto PDMS. Due to the hydrophobicity of PDMS, water droplets do not wet its surface. Even when the surface is chemically treated to become hydrophilic, water droplets form rings during the drying process. Additionally, if the previous droplet has not entirely dried, a coalescence of droplets occurs, in which case non-uniformities appear. It can be minimized by heating the substrate to enhance evaporation. Lastly, nanomaterials formed on the surface of PDMS do not adhere well and form cracks if the PDMS is stretched. Additionally, nanoparticles usually require sintering to become highly conductive, in which case cracks become evident upon stretching.

2.3.8. Drop-Casting

Drop-casting has been employed to deposit ink on a variety of substrates. A formulated ink is simply dropped on the sensing region and allowed to dry through evaporation of the solvent. Chemical, biological, and electrochemical sensors are usually fabricated with this method. The stability of the deposited material is highly dependent on the interaction between ink and substrate. In addition, on evaporation, the deposited material may not form a uniform layer.

With the drop-casting method, carbon nanocoils were deposited on a liquid crystal polymer substrate to fabricate a humidity sensor that achieved record response and recovery times of 1.9 s and 1.5 s, respectively. The hydrophobic nature of the liquid crystal polymer caused weak adsorption of water molecules on the sensor, which resulted in fast recovery upon desorption of water molecules [46]. Drop-casting was also employed to deposit graphene oxide (GO) onto water-transfer paper to fabricate a strain sensor/actuator for detecting throat motion and emitting the respective sounds. First, GO dispersion was drop cast onto water-transfer paper and dried, followed by laser-scribing a defined region in order to reduce the graphene oxide (rGO). Then, the paper was immersed in deionized water to wash off unreduced graphene, leaving only rGO supported on a poly(vinyl alcohol) (PVA) film, which was used as a sensor to detect skin motion [15].

2.3.9. Patterning Methods

In addition to the deposition of nanomaterials onto substrates and bulk mixing to form nanocomposites, many applications require patterning of the nanomaterials. Inkjet printing has the ability to deposit and pattern nanomaterials in a single step, but other methods require a combination of pre- or post-patterning. Laser ablation is a technique used to define patterns onto a flexible substrate such as PET. A focused laser delivers high optical energy to the substrate, thereby breaking up the molecular bonds and evaporating the molecules in the gaseous form [79]. A conductive CNT/PDMS nanocomposite is then poured into the grooves, and the extra amount is removed by a blade. Another plain PDMS layer is coated on top of the patterns and finally cured. Upon debonding, relief structures of conductive CNT/PDMS were formed onto a bulk PDMS. The laser ablation method forms extruding features without any masks, stamps, or lithography steps while achieving feature sizes as small as 20 μm on PET substrate. Similarly, micromilling can be used to define features on a plastic substrate, such as acrylic, with a minimum feature size of 30 µm [42]. Micromilling uses milling bits (endmills), which are capable of cutting the substrate both axially and laterally. A variety of flexible materials can be used as substrates, and it is most suited to fabricating molds [80].

2.4. Summary

In summary, several methods have reported to deposit and pattern carbon nanotubes on PDMS. Spray coating takes advantage of the solution processability of carbon nanotubes in aqueous solutions. It deposits over a large area, but requires additional patterning. Transfer techniques usually require some form of photolithography or micromachining prior to CNT transfer. Filtration methods also require a post-patterning step. The highest conductivities were achieved with the use of single-walled carbon nanotubes and with minimum impurities.

High-quality dispersion of carbon nanostructures in water is important for several reasons, for example, to avoid the use of toxic organic solvents, obtain low cost and low complexity formulations, and attain compatibility with biomolecules, etc. However, due to the hydrophobic interactions in water, graphene and carbon nanotubes agglomerate, which hinders the direct dissolution of those materials in water. Therefore, alternative aqueous dispersions are being developed. Georgakilas *et al*. [81] developed a carbon-based ink in which no surfactants or hydrophilic polymers were necessary for dispersion. The carbon nanotubes were made hydrophilic by functionalization with dihydroxy phenyl groups and subsequently added to the exfoliated graphene. The stabilization of graphene by carbon nanotubes in aqueous solution occurred by preferential trapping of carbon nanotubes between graphene sheets or modification of graphene edges. The solution was stable and achieved a minimum sheet resistance of 25 Ω/sq.

Most commercial carbon nanotubes are available in the form of powder or dispersed into solvents. For powder-based carbon nanotubes, dispersion in water requires the use of a surfactant or chemical modification [20]. Nevertheless, due to the low electrical conductivity of surfactants, the final conductivity of the printed film is impaired, so that the remaining surfactant molecules are regarded as undesired impurities. Therefore, patterning inks of carbon nanomaterials still presents challenges, especially for low cost and low complexity fabrication of sensors.

CHAPTER 3. TRANSFER PRINTING OF CARBON NANOTUBES TO PDMS

3.1. Introduction

The inkjet printing technology works well for printing on substrates that readily absorb the solvent, such as paper. However, for substrates that do not absorb the solvent, the droplets should be allowed to dry before printing an adjacent droplet to minimize coalescence and the coffee ring effect. In what follows, the main issues are defined, and our method to avoid such problems is described.

3.2. Issues of Inkjet Printing Carbon Nanotubes Directly on PDMS

For the fabrication of sensors, a flexible and stretchable material offers lower resistance to stretching. In addition, for wearable sensors, the materials should be biocompatible. PDMS is one of the best candidates that meet these criteria because it can be easily fabricated, is biocompatible, and can be stretched by more than its length. Although PDMS alone does not conduct electricity, it is possible to fabricate conductive nanocomposites by embedding a material that is conductive, for example, carbon nanotubes.

Carbon nanotubes are a class of materials suitable to be conductive fillers in a PDMS matrix. They have proved to be highly conductive [82], can be synthesized in high quantities, and are solution processable. Due to their high aspect ratio, they have a lower percolation threshold compared to nanoparticles. That means they conduct electricity even at low concentration inside a polymer matrix. Therefore, they are preferred over silver nanoparticles or carbon black [59].

Part of this chapter was previously published as T. H. da Costa and J.-W. Choi, "Low-cost and customizable inkjet printing for microelectrodes fabrication," Micro and Nano Systems Letters, vol. 8, art. 2, 2020. doi: 10.1186/s40486-020-0104-7. Reprinted by permission of Springer Nature.

Due to the nanometer size of carbon nanotubes, it is possible to process them with solutions. Without using a solution, the carbon nanotubes can be used as-grown, which means in their pristine form. Optionally, they can be transferred to another substrate via PDMS casting. However, without post-treatment to remove impurities, their use is significantly reduced. Also, patterning is complex because it requires patterning of the metal seeds using lithography or other micromachining equipment.

Inkjet printing is a low cost, low complexity method of printing nanomaterials dispersed in solution. It does not require the use of stencils like screen printing, or complex fabrication masks such as photolithography. However, one of the issues of printing a dispersion of solids is the coffee ring effect. The droplet, which is deposited on the substrate, has a pinned contact line. Evaporation occurs more quickly at the edges of the droplet than at the center, forming a capillary flow outwards to replenish the evaporated liquid, which makes the solid content to move to the edges of the droplet, thus forming a coffee ring [83]. Additional issues are the irregular wetting on the substrate, bulging of the printed patterns, and agglomeration of adjacent droplets [84].

3.3. Experimental Details of the Transfer Printing Method

3.3.1. Ink Solution Preparation

Ink development is an important step for successful inkjet printing. Aqueous solutions are well suited to cartridges, compared to organic solvents. Some organic solvents also solubilize carbon nanotubes, but they are toxic and may damage the cartridge. On the other hand, carbon nanotubes agglomerate in aqueous solution, so a surfactant is used to provide a stable dispersion.

Through extensive testing of organic solvents, it has been found that carbon nanotubes can be dispersed in organic solvents. Liu and Choi [85] found a reaggregation of MWCNT after 70 hours in the order: toluene > chloroform > THF > DMF. DMF was found to be the best dispersant of MWCNT among the ones tested. However, chloroform was found to be the best common solvent when PDMS and MWCNT are mixed. Acetone has been used as a solvent for SWCNT by Lau et al. [86], but the quality of the dispersion was not reported. In that study, it was found that the solvent influenced the hardness and flexural strength of the epoxy composite (due to unreacted epoxide groups and extent of cure reaction). In addition to dispersing SWCNTs with acetone only, Gong et al. [87] added an anionic surfactant (polyoxyethylene 8 lauryl) to improve CNT dispersion in acetone. Briefly, polyoxyethylene 8 lauryl was dissolved in acetone, and carbon nanotubes were added to the as-prepared polyoxyethylene 8 lauryl solution. Then epoxy and hardener were added to the mixture to provide a viscous suspension. The formulation, therefore, provided a polymer composite in the form of a paste from which the mechanical properties were studied. It contrasts to the liquid ink that is necessary for inkjet printing.

Tortorich et al. [77] used a solution of sodium n-dodecyl sulfate (SDS) and water to disperse carbon nanotubes. Like polyoxyethylene 8 lauryl, SDS is also an anionic surfactant, which indicates the possibility to disperse carbon nanotubes with acetone and SDS. However, the use of acetone to disperse carbon nanotubes is advantageous only if no surfactant is necessary. If a surfactant is needed, then the advantage of using acetone is lost, in which case an aqueous solution can be used with the help of a surfactant. To determine if acetone alone can be used to disperse carbon nanotubes, 45 mg of MWCNT were added to 4.5 ml of acetone in a vial and sonicated for 30 minutes. For comparison, 45 mg of MWCNT were added to 4.5 ml of deionized water in a separate vial and sonicated for 30 minutes. It was observed that without the use of SDS aggregation of MWCNTs occurred both in acetone and water during and after sonication

(Figure 1a). With the use of SDS, aggregation of MWCNTs occurred only in acetone (Figure 1b). On the other hand, with SDS in water, the MWCNT dispersion was stable at least for ten days.

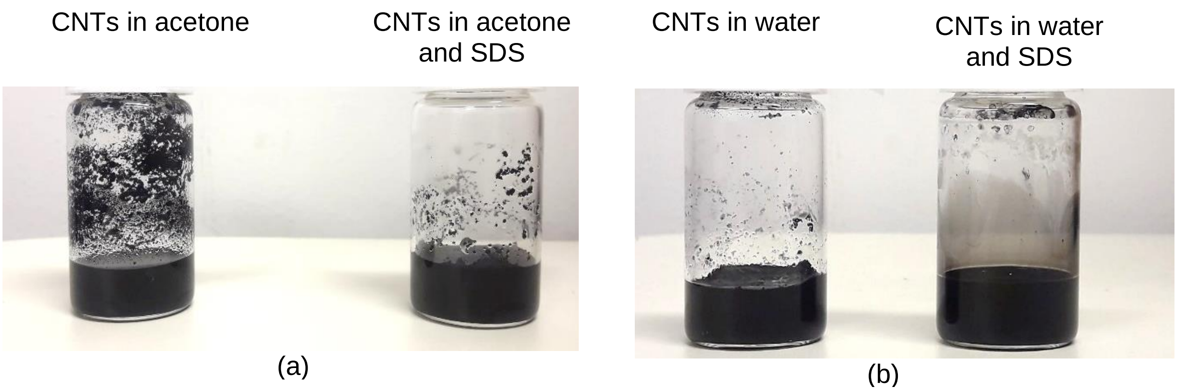

Figure 1. Comparison of dispersing agents for multi-walled carbon nanotubes (MWCNT) after sonicated: (a) MWCNT in acetone alone and deionized water alone. Sonication of MWCNT and acetone alone does not provide a stable dispersion. The same is valid for MWCNT and water alone, and (b) MWCNT with SDS in acetone and MWCNT with SDS in deionized water. A stable dispersion was found only in MWCNT with SDS in deionized water. The composition was 45 mg of MWCNT, 31.5 mg of SDS, and 4.5 ml of acetone or water in each vial.

The optimal formulation for inkjet printing on PET film has been previously developed in our group [77]. For the ink preparation, 10 mg/ml of MWCNT (Cheap Tubes Inc., Brattleboro, VT, USA) and 7 mg/ml of SDS (Alfa Aesar, Ward Hill, MA, USA) were added to 5 ml of deionized water in a vial, sonicated for 30 minutes at 80 W in a bath sonicator (Fisher Scientific FS20D), transferred to centrifuge tubes and centrifuged for 5 minutes at 12,000 rpm. The supernatant was recovered and directly injected into a cartridge. The inkjet printer used was an HP Envy 4501 with a corresponding cartridge for the printer. The cartridge was opened and thoroughly cleaned before the addition of the carbon nanotube ink.

3.3.2. Transfer Printing Process

Patterns were printed using an office inkjet printer (Figure 2a). One of the challenges of using water-based ink is to find a suitable substrate that quickly absorbs the ink, in order to have a sharp pattern characteristic and to avoid the coffee stain effect [66]. To minimize those issues, carbon nanotubes were inkjet-printed onto a PET film and subsequently transferred to PDMS. To this end, a PET film designed for inkjet printing (Inkpress ITF851150) was used. Patterns were printed several times to improve the uniformity of the film and reduce the sheet resistance. It was observed that electrical conduction started at five prints. For the PDMS preparation (Sylgard 184), the PDMS base was thoroughly mixed with a curing agent (weight ratio 10:1) and placed in a vacuum for 20 minutes to remove air bubbles.

PDMS was then spin-coated on the samples and cured at 90 °C for one hour (Figure 2b). The spin coating procedure comprised of ramping up the speed at 300 rpm/s to allow uncured PDMS to spread over the substrate, then maintaining the desired speed until the total time was 90 seconds. Such a relatively long spinning time ensures that all the uncured PDMS gets thrown off the substrate. The ramp down of the speed was set at 500 rpm/s for 10 seconds. Using the described procedure, PDMS films with thickness of 300 µm were obtained at the speed of 250 rpm. The top PDMS layer was then peeled off, containing the CNT patterns (Figure 2c). Finally, a sensor was assembled by bonding three layers of the horizontal and vertical CNT patterns (Figure 2d). The middle layer of PDMS provided isolation between the top and bottom CNT patterns, while the top PDMS provided passivation of the device. Here, PDMS layers were bonded by the corona discharge method. Briefly, by applying a strong electric field (one cm away from the surface for one minute), silanol groups are created at the surface, which upon touch with other PDMS layers, creates a permanent bond [88]. Finally, to provide a permanent bond, the sample was heated at 90 °C for one hour.

Using the transfer printing process described above, two types of sensors were fabricated: (i) a single carbon nanotube line that works as a force-sensing resistor and (ii) a two-dimensional force sensor composed of multiple lines of carbon nanotubes, having the capability to map force application in two dimensions. The single line sensor required only two layers of PDMS, whereas the two-dimensional sensor required the third layer. Therefore, after bonding the middle layer, its top surface was also corona-treated, and the third layer was assembled, forming a three-layer device.

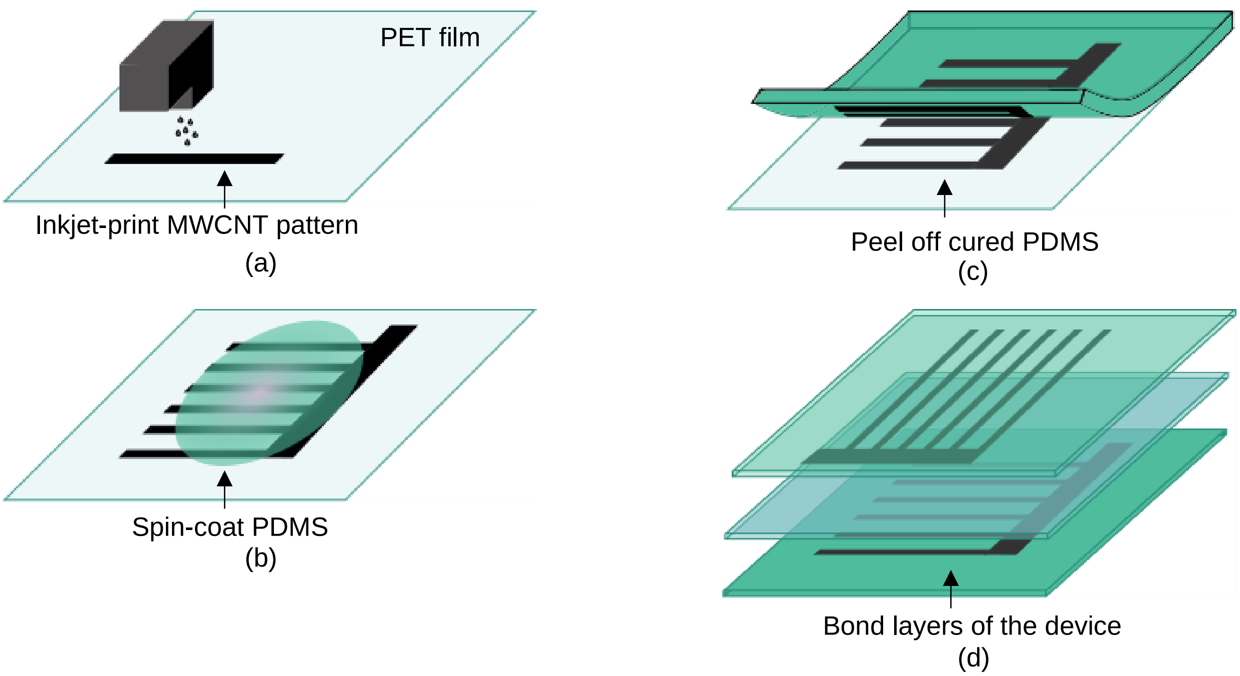

Figure 2. Inkjet and transfer printing carbon nanotube patterns: (a) inkjet-print MWCNT ink onto PET film using an office printer; (b) spin coat PDMS on the patterns and cure PDMS; (c) peel off PDMS containing CNT patterns, and (d) bond layers of the device.

For sheet resistance measurements, patterns with dimensions of 10 mm × 10 mm were printed on PET sheet from 5 to 35 times and subsequently transferred to PDMS. The sheet resistance was obtained with a four-point probe method.

3.3.3. Characterization of the Printed Film on Transparency

Uniformity

The uniformity of CNTs on PDMS was verified with SEM (scanning electron microscopy) images. As shown in Figure 3, the microscopic uniformity of MWCNT was achieved on PDMS with the transfer printing method.

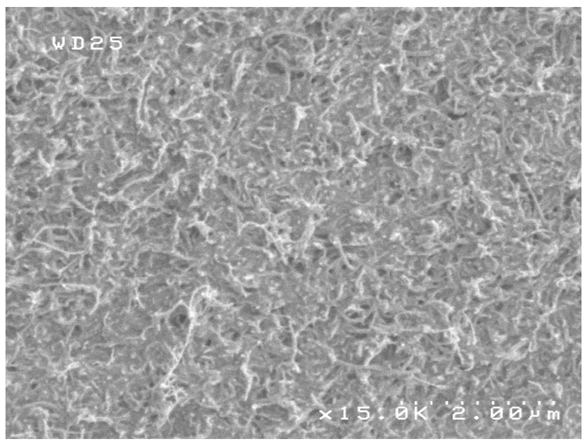

Figure 3. SEM image of inkjet-printed MWCNTs on PDMS. Microscopic uniformity was achieved with the transfer printing method.

Resolution

Due to the requirement to print several times, at each print, the office inkjet printer adds misalignment. Therefore, the minimum spacing between two lines of CNTs obtained was 1 mm, while the minimum line width was 0.8 mm. The use of an office inkjet printer allows the deposition of large-area patterns at the expense of pattern resolution.

Sheet resistance

Due to the electrical conductance of carbon nanotubes, each carbon nanotube provides a conductive path for current to flow. As more carbon nanotubes are present in a film, more conduction paths are available. For a single print, only sparse carbon nanotubes are printed. But for more prints, the film becomes thicker, thus offering less resistance to electric current. Therefore, the sheet resistance decreases with an increasing number of prints. This is evidenced in Figure 4. In addition, the ratio of the sheet resistances provides a measure of the transfer efficiency. Equal resistances means that all the CNTs have been transferred from PET to PDMS.

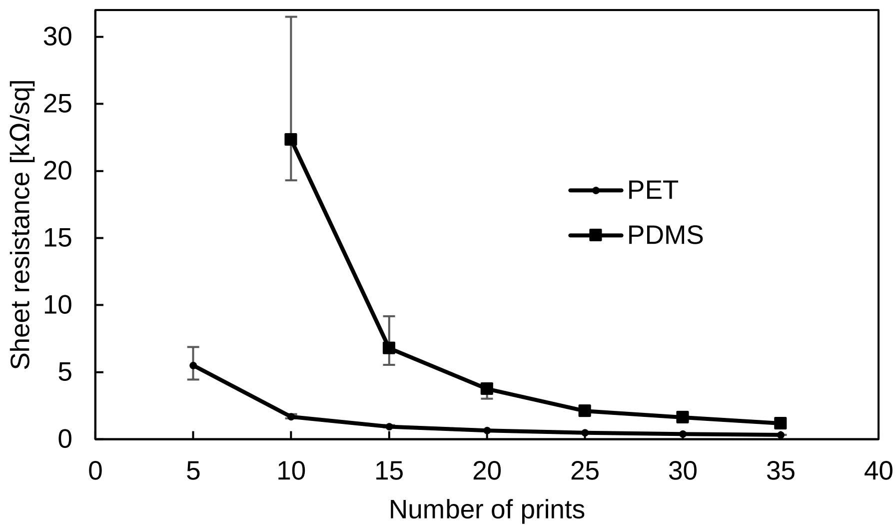

Figure 4. Sheet resistance of CNTs on PET film (inkjet-printed) and PDMS (after transfer from PET). The sheet resistance decreases as the number of prints increases. The lowest sheet resistance on PDMS was 1.2 kΩ/sq when printed 35 times.

Other factors that influence the resistivity are the CNT and SDS concentrations [77], since the weight percentage of CNTs is directly related to the percolation of the CNT network (*i.e.*, the degree with which a conductive path is formed) because a solution containing higher CNT weight percentage will deposit more CNTs. Also, the resistivity is affected by the concentration of SDS, which bonds to the CNT surface to prevent the bundling of CNTs. The use of SDS as a surfactant is required, but the downside is lowering the ability of CNTs to make electrical contacts with other carbon nanotubes.

Thickness

Each CNT has a diameter of tens of nanometers, and they are deposited mostly horizontally at each print, so the CNT film should have a few hundreds of nanometers. However, for practical verification, the sheet resistance is a better tool than the thickness. The number of prints is the controllable variable for the inkjet printing deposition process, such that one layer of CNT is added to the film at each print. In that case, the desired sheet resistance of the CNT feature can be directly related to the necessary number of prints. The sheet resistance was verified to decrease as more prints are performed, as shown in Figure 4.

3.3.4. Removal of SDS

Several authors have indicated the removal of SDS after printing [89]. SDS is soluble in water, so running water solubilizes SDS molecules attached to the surface of the film. In addition, it has been reported that water and diluted nitric acid were used in the removal of SDBS from SWCNT [73]. Rinsing in distilled water [90] and immersion in nitric acid were also performed to remove SDS from SWCNT, which improved sheet resistance with negligible chemical doping of CNTs [89]. However, the reflux in nitric acid actually functionalized MWCNT creating carboxyl, hydroxyl, and carbonyl groups at the defect sites [72]. In addition, De Nicola *et al.* [91] rinsed MWCNT-SDS dispersion in a solution of ethanol, methanol, and water (proportion of 15:15:70 to remove surfactant after being printed). In spite of the previous reports indicating a washing step in water to remove the surfactant, washing experiments performed on the inkjet-printed MWCNTs on PET film did not show any improvement in the sheet resistance. In addition to a rinsing step with water, isopropyl alcohol (91%) was jetted directly at the printed CNT patterns on PET film to remove SDS, however, no improvement in sheet resistance was observed.

3.3.5. Method of Immersing the PDMS Into Acetone

During the process of peeling off PDMS from PET film, if the PDMS membrane thickness is lower than ~100 µm, PDMS may tear because the pulling tension required to separate the PDMS from the PET is greater than the tension that the PDMS is capable of withstanding. For those cases, a method was developed to obtain PDMS membranes as thin as 30 µm without any tearing. The sample was immersed into acetone for 5 seconds (until the PDMS layer becomes transparent, which indicates that acetone has diffused through PDMS), and peeling was performed while the sample was immersed. Acetone is a polar solvent that diffuses into PDMS while it is immersed. Acetone reduces the adhesion energy of PDMS-PET film, effectively reducing the pull tension necessary to separate PDMS from PET film. The pulling tension is much lower when immersed into acetone, than when not immersed. By using this method, it was possible to peel off PDMS membranes as thin as 30 µm.

3.3.6. Thermal Processing of the PET Film

The transfer printing method shown thus far has been successfully employed to transfer carbon nanotubes from PET film to PDMS. However, in order to improve the consistency and sheet resistance of the final patterns on PDMS, the PET film was thermally treated before peeling off the PDMS from PET. The complete procedure consisted of inkjet-printing a CNT pattern onto PET film, spin-coating PDMS on top of the CNT pattern to form the diaphragm, and curing the PDMS. Before peeling off PDMS from the PET film, heated air was applied directly on the PET film with the aid of a solder rework station (air gun). The air temperature was set at 300 °C, and the distance between the air gun and the PET film was 3 cm at the onset of the procedure. The air gun was then brought closer to the PET film, until reaching a distance of 0.5 cm from the PET film. The duration of the procedure lasted 120 seconds.

PET has a melting temperature around 260 °C [92], but PDMS does not melt at that temperature. It has been reported that the thermal decomposition temperature of PDMS is around 310 °C [93], so that applying a temperature below 310 °C does not adversely affect the PDMS membrane. Applying a thermal treatment to PET just above its melting point (260 °C) turns the PET soft and viscous, while the PDMS does not melt due to its cross-linked nature [94]. Thus, the thermal treatment procedure allows the easy separation of PDMS from PET. The visual inspection of the transferred CNTs to PDMS shows a darker pattern after thermal treatment in comparison to no thermal treatment (Figure 5).

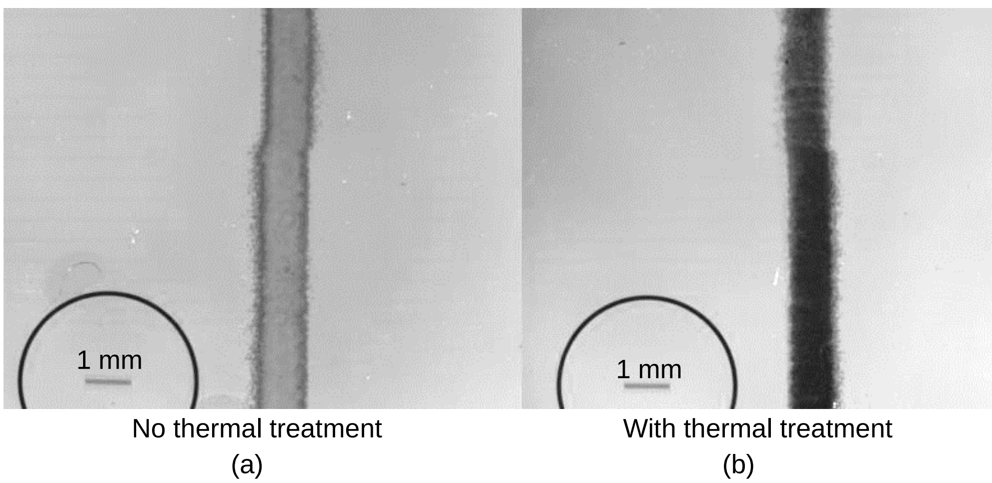

Figure 5. Comparison of carbon nanotube patterns after transferred from PET to PDMS: (a) PDMS was simply peeled off from PET, and (b) PDMS was peeled off after applying heat on the PET side. The thermal treatment reduced the resistance of the carbon nanotube line from 683 kΩ to 50 kΩ.

Moreover, the thickness at which the PDMS tears apart while peeling off from PET is 300 μm (with no thermal treatment). On the other hand, with thermal treatment, diaphragms with thicknesses lower than 30 μm were successfully peeled off without tearing. The resistance of

CNT patterns was measured for a demonstration of the improvement produced by the thermal treatment method. In the first case, the resistance of inkjet-printed CNTs directly on PET film showed an average of 13 kΩ and a standard deviation of 0.4 kΩ. In the second case, the resistance of transferred CNTs to PDMS after thermal treatment showed an average of 50 kΩ and a standard deviation of 6.5 kΩ. In the third case, the resistance of transferred CNTs to PDMS without thermal treatment showed an average of 683 kΩ and a standard deviation of 129 kΩ. In each case, ten different samples were measured. The thermal treatment, therefore, improved the transfer of carbon nanotubes from PET to PDMS, since it was observed an improvement of 92.7% in the resistance of the samples that were thermally treated.

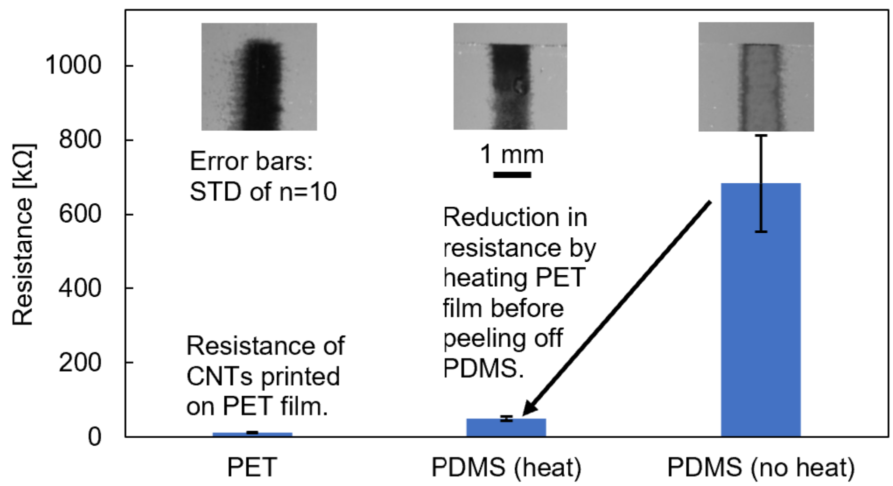

Figure 6. Comparison of the resistance of carbon nanotube lines on different substrates and with/without thermal treatment. The resistance of CNTs inkjet-printed on PET film is 13 kΩ, while on PDMS after thermal treatment is 50 kΩ, and on PDMS without thermal treatment is 683 kΩ. The improved method shows a reduction in the resistance from 683 kΩ to 50 kΩ. The dimensions of the lines were 28 mm x 1 mm (28 squares).

3.4. Development of a Custom Printer

Inkjet printing has seen tremendous development in the deposition of nanomaterials for the fabrication of microelectrodes. It has been considered as an alternative for printing nanomaterials in the applications of flexible electronics and point of care sensors. The superior properties of inkjet printing, such as solution processing and maskless printing, enable the technology to be used in a variety of applications. A common issue in the development of inkjet-printed sensors is the high cost of inkjet printing research equipment.

While many of the studies mentioned above used professional inkjet printers, some of them employed office inkjet printers, which are widely available at low cost. Office inkjet printers offer the advantage of printing large-area patterns with high speed, at the expense of lower resolution and lack of control of the quantity of material deposited.

Several approaches have been employed in the development of low-cost ink deposition processes. In microfluidic impact printing(MIP) [95], [96], a pin which is driven by an electromagnetic actuator strikes an elastic membrane. The ink contained in the microfluidic channel below the membrane ejects in the form of a small droplet. In electrohydrodynamic jet printing [97], a high voltage is applied between the print head and the substrate, which ejects ink from the nozzle onto the moving substrate to form a pattern. Printed lines can be achieved with widths as small as 700 nm. These approaches provide an alternative to standard printing procedures. However, they are not easily replicated since the cartridge and nozzle have to be microfabricated in both cases.

Here, a customized inkjet printer with comparable characteristics to advanced commercially available inkjet printers is presented, while being affordable by utilizing off-the-shelf components. Furthermore, it is capable of printing several nanomaterial solutions, including carbon nanotubes, graphene oxide, and silver nanoparticles. The capability of the printer was demonstrated by patterning carbon nanotubes on polymer substrates. The printer can easily be replicated and provides a foundation for the development of flexible and disposable sensors.

3.4.1. Development of the Inkjet Printer Stage

The inkjet printer consists of a moving stage, a print head with the cartridge, and a control board. An aluminum frame was used as the platform for the inkjet printer. The frame offers a large area of 35 cm x 35 cm for positioning the substrate, as illustrated in Figure 7a. The control board contains the microcontroller and two subsystems: a motor control for the positioning of the print head and a cartridge control that controls the ejection of droplets (Figure 7b). Stepper motors with a geared system providing 2060 steps per revolution were used for X and Y linear movements of the cartridge. Inkjet printer cartridges (HP C6602A) were thoroughly cleaned in deionized water and dried before use. The cartridge has a nozzle with an aperture of 55 µm (measured under an optical microscope) with a nominal average drop volume of 160 pl (obtained from the datasheet) [98]. Each droplet is generated by an electric pulse of 21 V for five µs sent by the microcontroller to the nozzle (Figure 7c). This type of cartridge uses thermal technology to generate droplets.

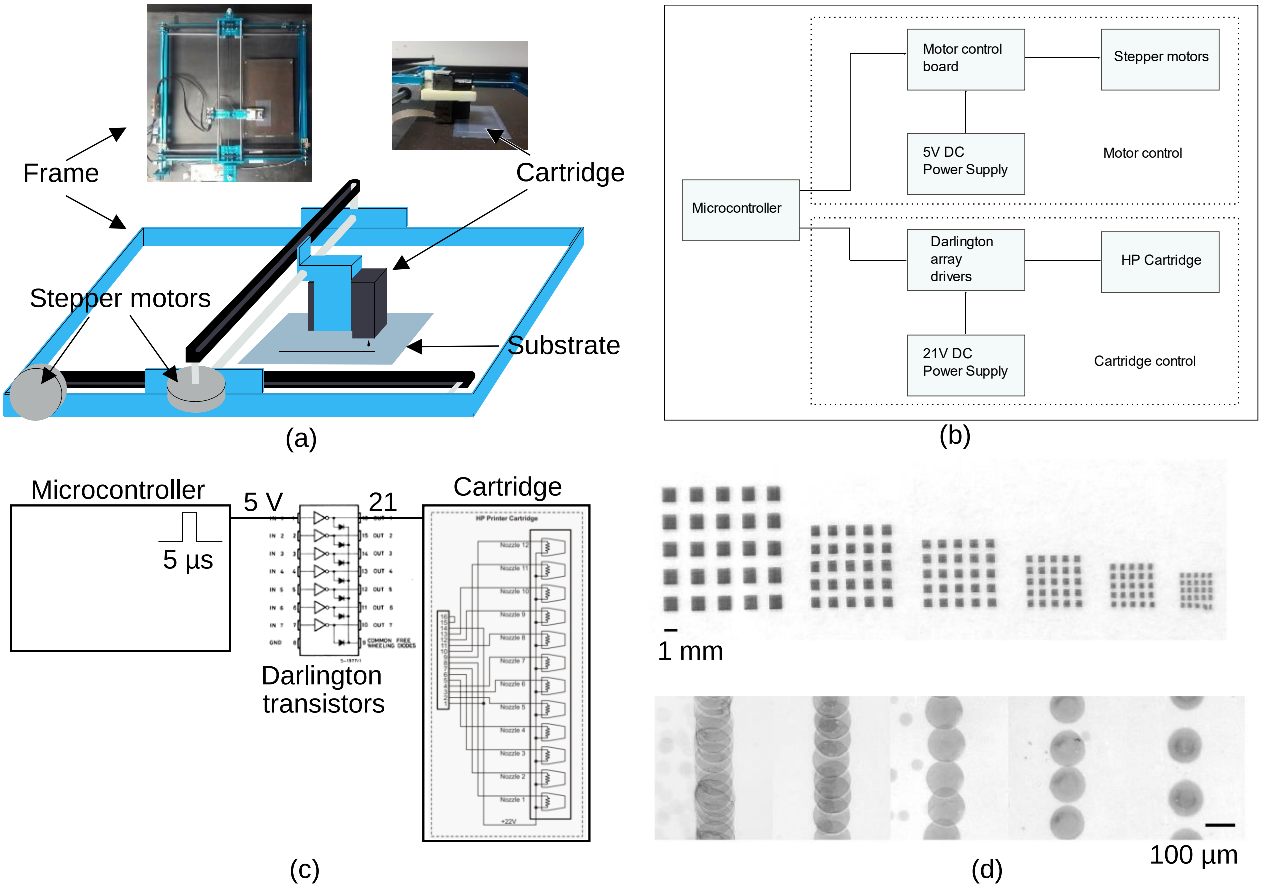

Figure 7. System schematic and customized patterns: (a) XY stage containing the print head and cartridge; (b) schematic of the control board; (c) the microcontroller sends voltage pulses of 5 µs of duration and 21 V of amplitude to activate a particular nozzle, and (d) carbon nanotube patterns printed on a poly(ethylene terephthalate) (PET) film (scale bar: 1 mm, above) and a single line of carbon nanotubes with different spacing between drops (scale bar: 100 µm, below).

When a voltage pulse is sent to the nozzle, a thin-film resistor in the nozzle heats to a high temperature, creating bubbles and ejecting the ink [66]. Line patterns with width as low as 120 µm and square patterns were printed on poly(ethylene terephthalate) (PET) substrate to demonstrate the characteristics of the printer (Figure 7d).

3.4.2. Characterization of the Custom Printer

For the characterization of the inkjet printer, PET sheets (Inkpress ITF851150) were cut into 70 mm x 50 mm and used as the substrate. In order for the substrate to maintain flatness during printing, it was attached to a glass slide, which was previously coated with poly(dimethyl siloxane) (PDMS). All measurements of dimensions were performed under a stereomicroscope (Leica MZ16), while sheet resistances were measured with a custom four-point probe setup. The current low-cost inkjet printer does not contain a heating stage, so the experiments were performed at room temperature. Alternatively, a heating stage would allow the improvement of the evaporation rate of the droplets. The carbon nanotube ink used to characterize the printer consisted of a stable dispersion of MWCNT (10 mg/ml) and SDS (7 mg/ml) in deionized water, as described in section 3.3.1.

3.4.3. Performance of the Custom Printer

Drop spacing

For performance testing of the developed printer, a single nozzle was used. The advantages are high spatial resolution and control of the number of droplets. The position of the cartridge is controlled by stepper motors. Each step of the motor corresponds to the minimum distance between drops printed on the substrate. Due to the reduction gears of the stepper motors, a single step corresponds to 18 µm, two steps correspond to 36 µm and so on. The spatial resolution of the inkjet printer is the smallest lateral displacement of the nozzle achievable for a single motor step, corresponding to a resolution of 18 µm (1412 dpi). In Figure 8, lines of carbon nanotubes were printed on PET film to determine the drop spacing. The points represent the average for each number of steps, while the error bars represent the standard deviation of the distance between adjacent drops for 20 times of printing (n=20). The deviations of the droplets both in the direction of the line and laterally were measured to obtain the positioning repeatability, achieving a standard deviation (SD) of 10.3 µm and 5.01 µm, respectively. The deviations can be attributed to the differences in trajectories of the ejecting droplets, which are mainly affected by the distance between the nozzle and the substrate.

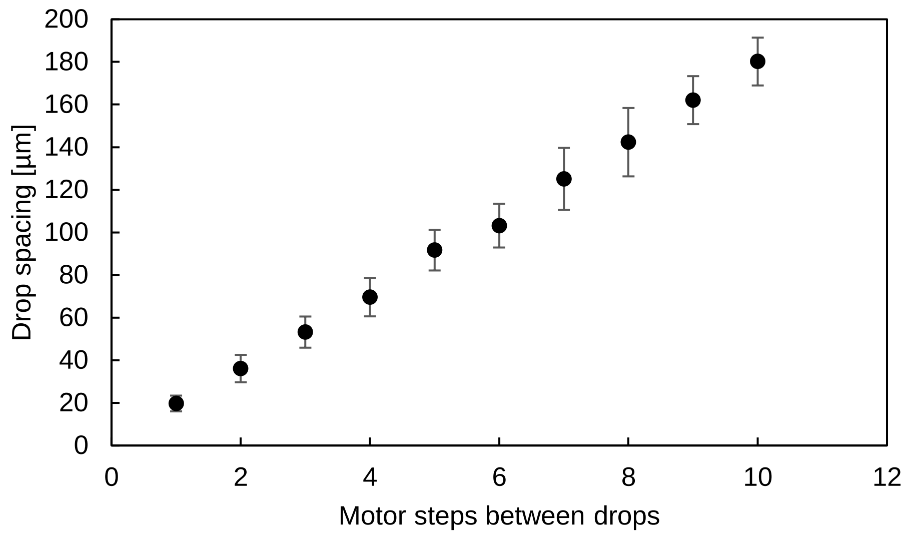

Figure 8. Drop spacing measurement of the custom printer. Carbon nanotube lines were printed with each line having a different number of motor steps between drops. Each step of the motor, therefore, corresponds to 18 µm. Error bars show the standard deviation of 20 measurements.

Line width

When printing a single line of nanomaterial on the substrate, adjacent drops in close proximity produce an increased line width. Figure 9 shows the dependence of line width on the drop spacing. If the spacing between each drop is less than 70 µm, drops may overlap. When drops overlap, the resultant line width increases. But if the drops do not overlap, the line width is the same as the drop diameter. Several methods can be used to change the size of the printed droplet, such as modifying the nozzle diameter, changing the type of substrate, the ink formulation, and the hydrophilicity of the substrate to improve the wetting behavior [62]. In our experiments, changing the voltage and the pulse time did not affect the size of the printed droplet.

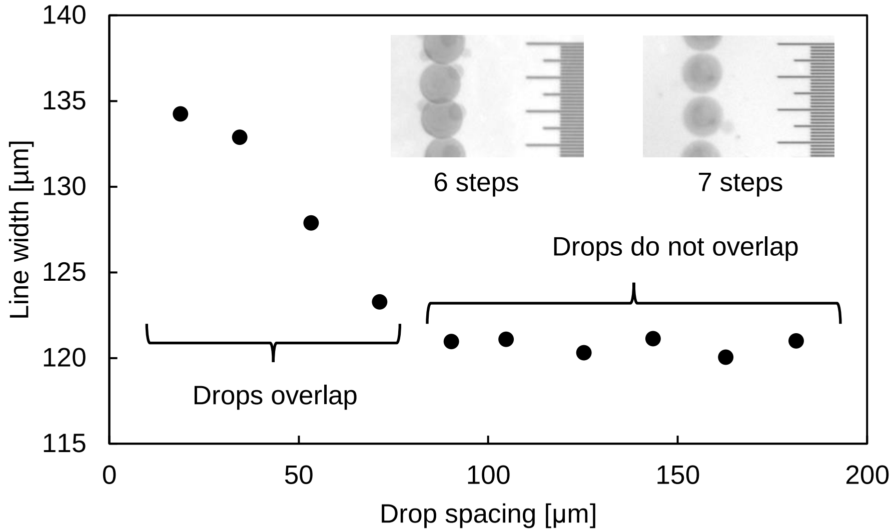

Figure 9. Line width dependence on the drop spacing. For small drop spacing, there is overlap, and the line width increases.

Sheet resistance

The conductivity of the printed patterns is essential when fabricating functional sensors. As can be seen in Figure 10, the measured sheet resistance is lower when drops are printed closer together. The reason is that if the drops overlap, more material is printed in a given area, which in turn decreases the sheet resistance. On the contrary, as the drop spacing increases, less material is printed in a given area, and the sheet resistance increases. If the drop spacing is greater than 90 µm, drops do not overlap, and a conductive path is not formed.

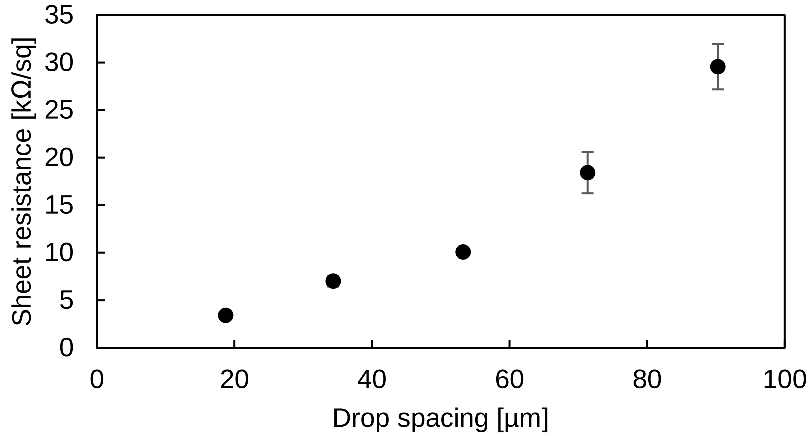

Figure 10. The sheet resistance of single lines of carbon nanotubes printed on PET. As the drop spacing increases, less material is printed in a given area, and the sheet resistance increases. Error bars show the standard deviation of ten measurements.

In Figure 11, square patterns of carbon nanotubes were printed on the PET sheet with dimensions of 10 mm x 10 mm. The measured sheet resistance decreases as a function of the number of prints due to more conduction paths being available for current to flow.

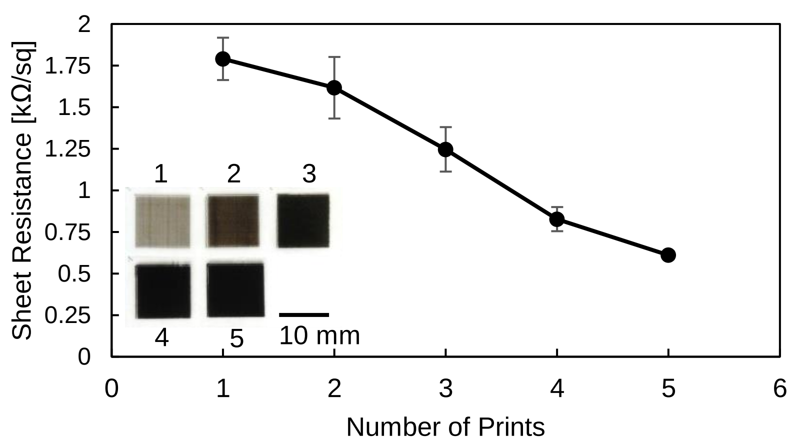

Figure 11. The measured sheet resistance of carbon nanotubes on PET printed from one to five times. Error bars show the standard deviation of measurements.

Table 3 shows the comparison of patterns deposited with a variety of inkjet printers and some representative performance parameters (sheet resistance, minimum line width).

Table 3. Comparison of inkjet printing performance.

Inkjet Printer	**Printed Material**	**Substrate**	**Sheet Resistance/Resistivity**	**Minimum Line Width**	**Ref.**
MicroJet	SWCNT	Glass	25 μΩ·m at 8 prints	150 μm	[99]
Canon BJC 4550	MWCNT	Transparency foil	40 kΩ/sq at 90 prints	200 μm	[72]
Micromech Systems	MWCNT	Glass	30 kΩ/sq at 1 print	98 μm	[100]
Microfab JetDrive III	MWCNT	PET film	0.7 kΩ/sq at 14 prints	100 μm	[101]
Dimatix DMP-8200	Ag nanoparticles	Paper	0.083 mΩ·m	59 μm	[102]
Custom (MIP)	Biological reagents	PDMS	N.A.	100 μm	[95]
Custom (EJP)	PEDOT/PSS, polyurethane	Silicon wafer	N.A.	700 nm	[97]
Custom	MWCNT	PET film	0.61 kΩ/sq at 5 prints	120 μm	This work

N.A.: Not available, PDMS: poly(dimethyl siloxane), EJP: electrohydrodynamic jet printing, MIP: microfluidic impact printing, SWCNT: single-walled carbon nanotube, MWCNT: multi-walled carbon nanotube, PEDOT/PSS: poly(3,4-ethylenedioxythiophene)/poly(styrenesulphonate).

3.5. Summary

In this chapter, to overcome the issues when inkjet-printing carbon nanotubes directly onto PDMS, a transfer printing method was described. Coffee ring effect and irregular patterning are the main issues that the transfer printing method addresses. The first step is to inkjet-print carbon nanotubes on a PET film, followed by spin coating PDMS over the patterns and curing the PDMS. Then, a thermal treatment is applied to release the PDMS from the PET film. The thermal treatment allowed more carbon nanotubes to be transferred to PDMS, compared to no thermal treatment, which reduced the sheet resistance of CNTs on PDMS by more than 90%. In addition, a cost-effective and customizable inkjet printer was developed, offering a resolution of 18 µm (1412 dpi) with the components available off-the-shelf, which is comparable to the advanced inkjet printers available for research. The inkjet printer was employed to print patterns of carbon nanotubes on PET film to demonstrate the capability of printing microelectrodes, which can be used in several applications such as electrochemical and humidity sensors.

CHAPTER 4. TWO-DIMENSIONAL FORCE SENSOR

4.1. Introduction

Flexible and stretchable sensors are gaining importance for applications in healthcare. For example, tactile feedback is one application in which the magnitude of the force is required, as well as its position in space. This requires a two-dimensional force sensor that provides such force information but also can be wrapped around the surface of the object and be comfortable to wear. This type of sensors is highly demanded in anthropomorphic prosthetic hands and robotics applications. To illustrate the sensing mechanism, first, a single line of carbon nanotubes was fabricated, and a force was applied perpendicularly to the line. It was shown the resistance change caused by the bending of the CNT line as well as the response of the sensor from the cyclic force application. Then, a two-dimensional force sensor with multiple lines was fabricated and characterized in terms of spatial distribution and sensitivity.

4.2. Force-Sensing Resistor Fabrication and Measurement

For the single line force sensor, the method of transfer printing described in Chapter 3 was used to obtain a single line of CNTs on PDMS (10 mm × 0.5 mm). First, carbon nanotubes were inkjet-printed onto PET film with an office inkjet printer. Then, PDMS was spin-coated, cured, and peeled-off from the PET film. This method resulted in carbon nanotubes being embedded in the PDMS layer. Then, electrical contacts were established with copper clips, and a passivation layer of PDMS (300 μm) was bonded to the first layer by corona treatment. The thickness of both PDMS layers was 300 μm, and an additional PDMS layer (4.2 mm) was placed below the

---

This chapter was previously published as T. H. da Costa and J.-W. Choi, "A flexible two dimensional force sensor using PDMS nanocomposite," Microelectronic Engineering, vol. 174, pp. 64–69, 2017. doi: 10.1016/j.mee.2017.02.001. Reprinted by permission of Elsevier B.V.

sensor to allow for deflection.

For testing the change in resistance upon compression force, the force-sensing resistor was tested in a testing machine (GeoJac Automated Load Actuator), as shown in Figure 12a. The linear actuator speed was set to 0.1 in./minute. The force applied was measured by a load cell (CNC Pacific Weighing), as depicted in the 3D model of Figure 12b, and the resistance was measured with a Keithley 2100 DMM. For the characterization of the sensor, the ball indentation experiment was employed [103]. In this experiment, a steel ball of diameter 12.7 mm (0.5 in.) descended with constant speed at the normal direction to the sensor, reaching the sample and creating an indentation into the sensor, which caused a strain on the carbon nanotube network, schematically depicted in Figure 12c. The ball stayed at maximum indentation for 5 s and then retreated to its initial position.

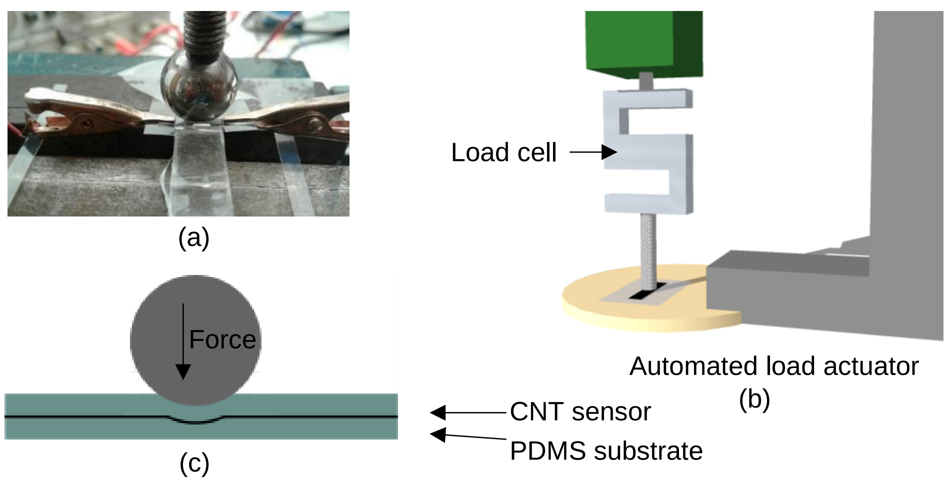

Figure 12. Testing of the force-sensing resistor: (a) picture of the ball indentation experiment; (b) schematic of the force applied by the steel ball, while a load cell reads the amount of force applied for calibration of the sensor, and (c) schematic of the strain generated by deflection.

Silicone oil was painted on the ball to prevent probe-sample adhesion. The resistance change for the experiment is shown in Figure 13. It was observed more than 20% change in resistance when the load was 0.5 N.

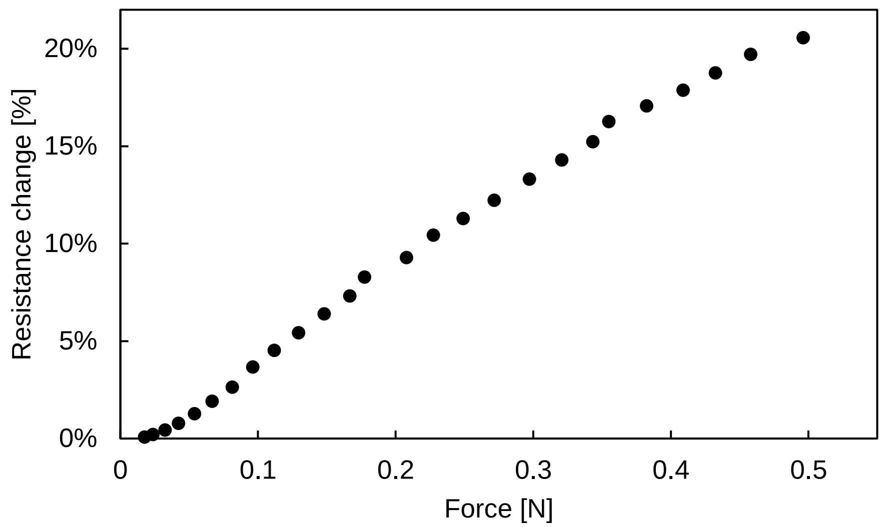

Figure 13. The resistance change of the force-sensing resistor. A ball indents the CNT line perpendicularly to the sensor. The resistance of the carbon nanotube pattern increases when the ball deflects the pattern.

The continuous operation of the sensor requires that the sensor be stable over time. A cyclic force application was performed to characterize resistance-time behavior. A similar procedure was applied as in the ball indentation experiment; however, with the repeated vertical motion of the ball. An automated system controlled the vertical speed of the ball. At each cycle, the ball touched the sample until the force reached 0.5 N (as measured by the load cell). After 5 s the ball retreated to the initial position. The resistance changed by 17% when the load was 0.5 N at each cycle, as shown in Figure 14. The stress relaxation is one of the characteristics of viscoelastic polymers. In the plot of Figure 14, it can be observed that the resistance level does not return to the original value, which could be ascribed to stress relaxation caused by the viscoelastic effect in PDMS. Such behavior has been further explored in previous publications [104], [105]. To mitigate those effects, the sensor was pre-loaded to a force higher than 0.5 N. Although the resistance does not return to the original value when a force is being applied, the difference between the peak and the base value of the resistance is representative of the magnitude of the force.

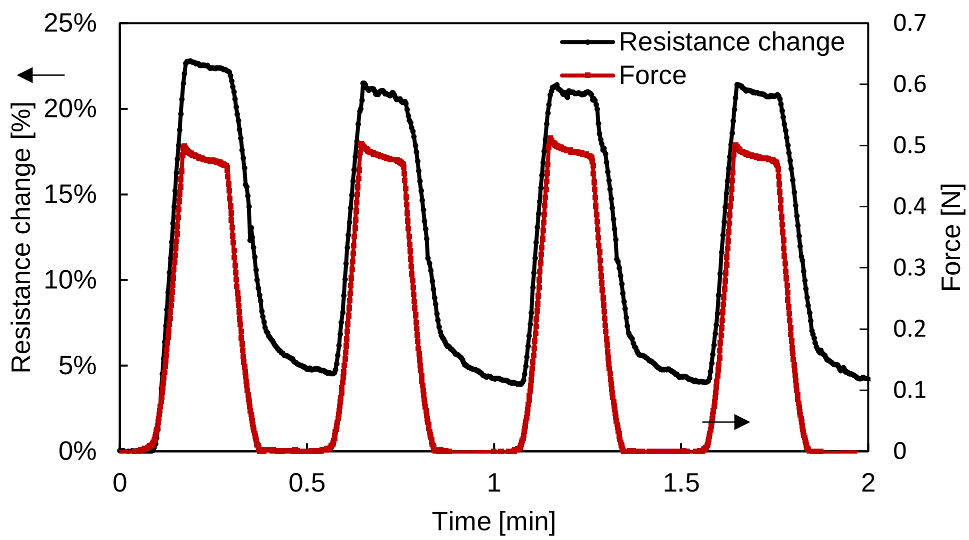

Figure 14. Resistance-time behavior of the CNT/PDMS force-sensing resistor when the load was applied cyclically to the sensor. The ball touched the sensor until force reached 0.5 N at each cycle, then retreating to the initial position after 5 s.

4.3. Two-Dimensional Force Sensor

The two-dimensional force sensor was fabricated by inkjet printing MWCNTs on PET film, spin-coating PDMS, peeling off the PDMS, and assembling the device. To obtain force distribution information, CNT lines were printed on the *x* axis and the *y* axis of the PET film. Then, PDMS was spin-coated on the whole film. Finally, the PDMS was peeled off and cut to obtain the top layer and bottom layer, as can be seen schematically in Figure 15a. The device was assembled with a separation layer of PDMS (300 µm thick), and the connections were secured with a snap-in connector. The assembled device with wire connections is shown in Figure 15c. Sixteen-channel analog-to-digital converters were connected to a microcontroller to provide resistance values from each of the CNT lines sequentially. Finally, an algorithm subtracted the value of resistances on the same line and adjacent to the point of interest, so that ghost-resistances were minimized. The program running in the microcontroller scanned for each value of the two-dimensional sensor and transmitted each value to a computer, which then plotted a near-real-time heatmap of the force.

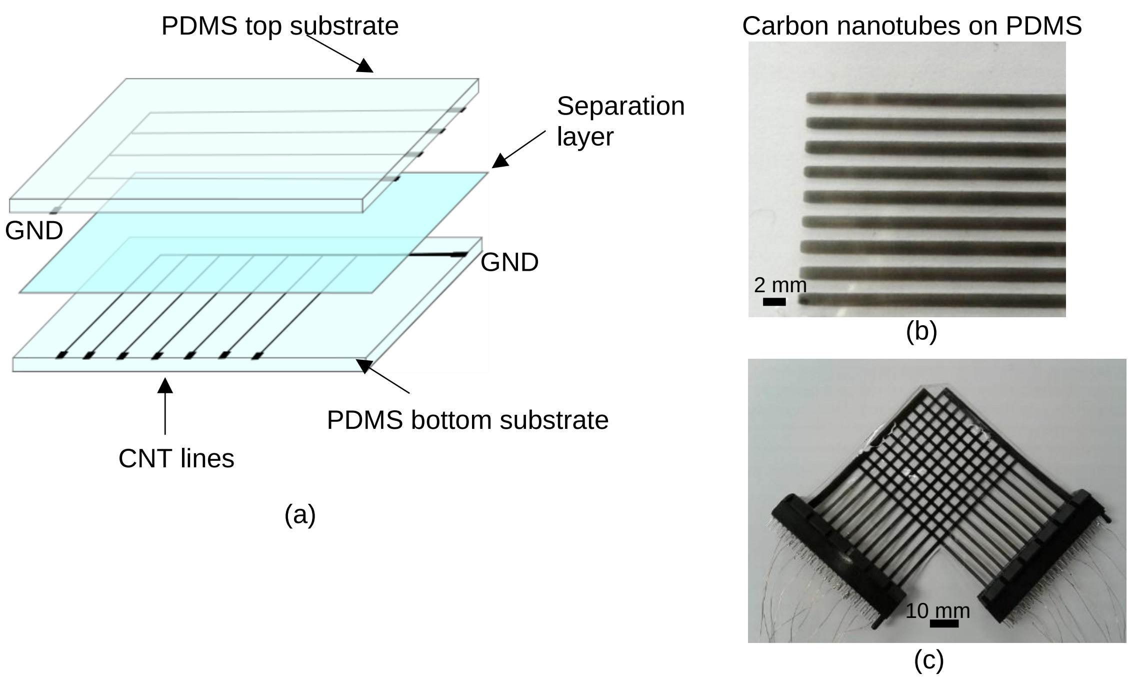

Figure 15. Fabrication of two-dimensional force sensor: (a) schematic of three layers of PDMS working as the top, separation, and bottom layers; (b) example of printing lines of carbon nanotubes on PDMS, and (c) sensor assembled.

The two-dimensional force sensor contains lines on separate layers. The lines were arranged perpendicularly to each other. Connections to CNT lines were established with the use of snap-in connectors. The initial resistance of each CNT line was measured to be ~300 kΩ, excluding the ground portion. A single voltage measurement was composed of the resistance of a single CNT line in series with a 300 kΩ resistor, thus forming a voltage divider. The output of this voltage divider was directly connected to an ADC, which has multiple inputs. Therefore, ten measurements were taken in the x direction and another ten measurements in the y direction. One measurement was taken in the beginning from all the inputs to establish the baseline, that is, with no force applied. Subsequent measurements were subtracted from the baseline value. When a force is applied at a particular position, the respective x and y resistances increase, which is observed at the ADC voltage reading. If there is no force application, the voltage reading stays constant, and the difference to the baseline is zero. The multiplication of corresponding x and y measurements provides the force information for a particular point. When all the points were measured, the corresponding values were plotted as a heat map on the computer. The heatmap and the respective picture of the force location are shown in Figure 16.

4.4. Discussion

The carbon nanotubes embedded in the polymer matrix form a conductive path. When strain is applied to the polymer, the number of contacts available for current to flow is decreased, therefore the resistance increases. The two-dimensional force sensor provides pressure feedback that closely mimics the human sensory system. Additional applications of the single line sensor are finger touch measurement and heartbeat monitoring. The inkjet printing is a simple, yet efficient way of patterning CNT/polymer composites. The method proposed here allows patterning of large-area networks of carbon nanotubes on PDMS, which has been difficult due to incompatibilities between PDMS and aqueous solutions. The demonstrated method avoids the use of masks or stamps and is well suited for low-cost BioMEMS devices and wearable sensors.

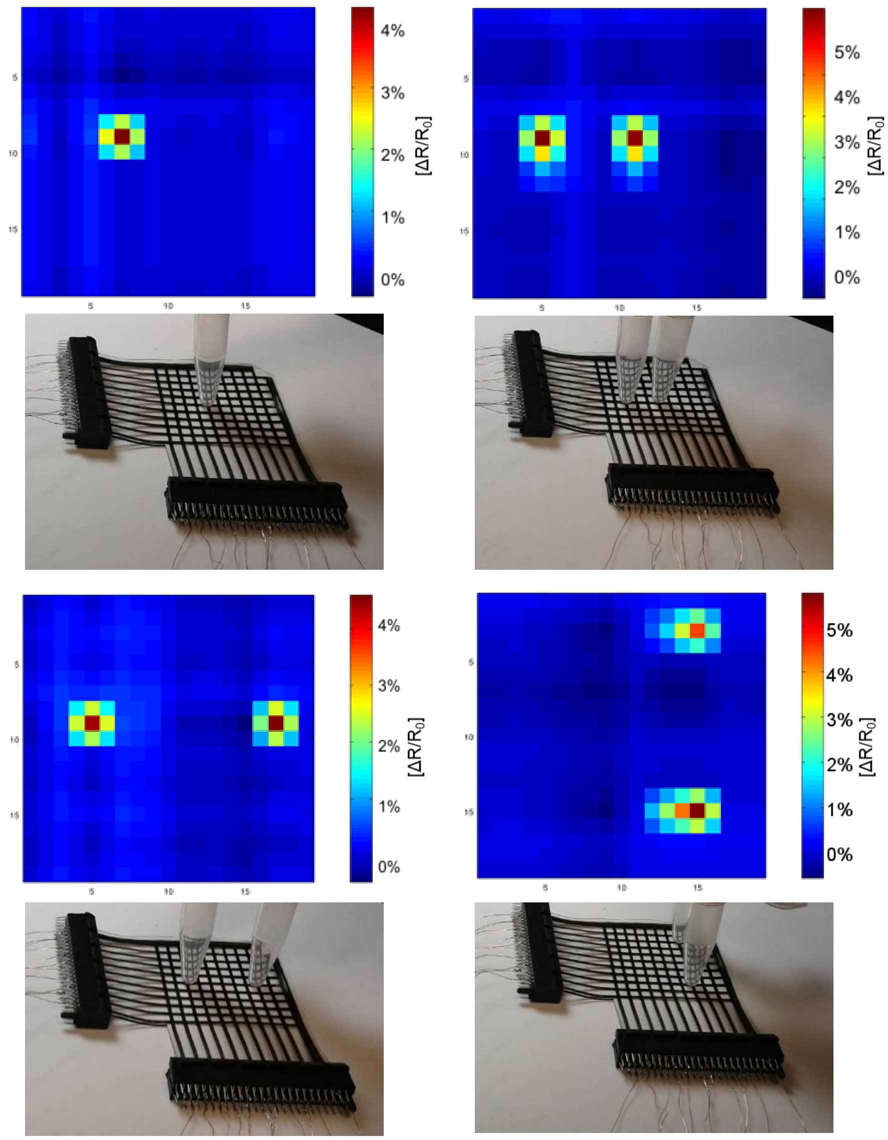

Figure 16. Two-dimensional force sensing with MWCNT/PDMS nanocomposite. The images show a single force application and multiple force application at different locations on the sensor.

4.5. Summary

In this chapter, applications of the transfer printing method are shown. The transfer printing method only utilizes an aqueous solution of carbon nanotubes with surfactant and is extremely simple, requiring only a few steps. First, the ink is printed on a PET sheet, and PDMS is spin-coated over the CNTs, which actively embeds the CNT film into PDMS. Subsequently, the

PDMS is peeled off, and the patterns are transferred to PDMS with high uniformity. The resulting composite is flexible and conforms to the surface. Through resistivity measurements, the electrical paths of the CNT network were verified, and SEM pictures showed that the pattern transfer maintains the CNT network after the transferring step. As a demonstration of the technology, an all-polymer flexible two-dimensional force sensor was fabricated and characterized, showing force mapping capability. The deflection of a single line of carbon nanotubes resulted in >20% change in resistance with 0.5 N of force applied perpendicularly to the CNT line. The repeated force application on the sensor showed an initial increase in resistance, and subsequent cycles followed the base value. In addition, the flexibility of the sensor allowed it to conform to a variety of non-flat surfaces, enabling the device to be used as a wearable sensor for pressure and force monitoring.

CHAPTER 5. PRESSURE SENSOR

5.1. Introduction

Pressure sensors are extensively used in the automotive industry, oil and gas industry, medical devices industry [106], and many others. The pressure is frequently the most important signal when monitoring the situation of the underlying process. In healthcare, many health conditions are characterized by abnormal pressure, such as high blood pressure and high intraocular pressure. Especially in medical care, the measurement of transpulmonary pressure is required during mechanical ventilation to prevent ventilator-induced lung injury [107]. Low limit of detection is important in many applications, as the air pressures range from zero to several hundred pascals. In addition, biocompatibility is desired so that the sensor can be worn by the user without causing adverse effects. Literature in pressure sensors often refers to the contact pressure exerted by force over an area, that is, $P = F/A$. However, the sensor reported here refers to the measurement of air pressure, both gauge pressure (in which the output is relative to atmospheric pressure) and sealed gauge pressure (in which the output is relative to a pressure set at fabrication time). The following sections provide the detailed fabrication procedure, the characterization of the pressure sensors and a discussion of their performance and advantages.

5.2. Fabrication Process of the Pressure Sensor

Two types of pressures can be measured with the fabricated pressure sensors, namely, gauge pressure (PSIG) and sealed gauge pressure (PSIS). In both cases, a pressure sensor is composed of two ports which receive pressure. The source port is connected to the source pressure, while the reference port is connected to a reference pressure. If the sensor is sealed, the reference pressure is the nominal pressure of the sealed chamber (PSIS) [108], which is determined at fabrication time. If the sensor is vented, the chamber has an open port which receives atmospheric pressure and one source port which receives source pressure [109]. Diaphragm pressure sensors with two configurations were fabricated; specifically, the gauge pressure sensor (open chamber) and the sealed gauge pressure sensor (sealed chamber).

The sealed gauge pressure sensor measures the pressure difference between the source pressure and the pressure inside the chamber (shown in Figure 17a).

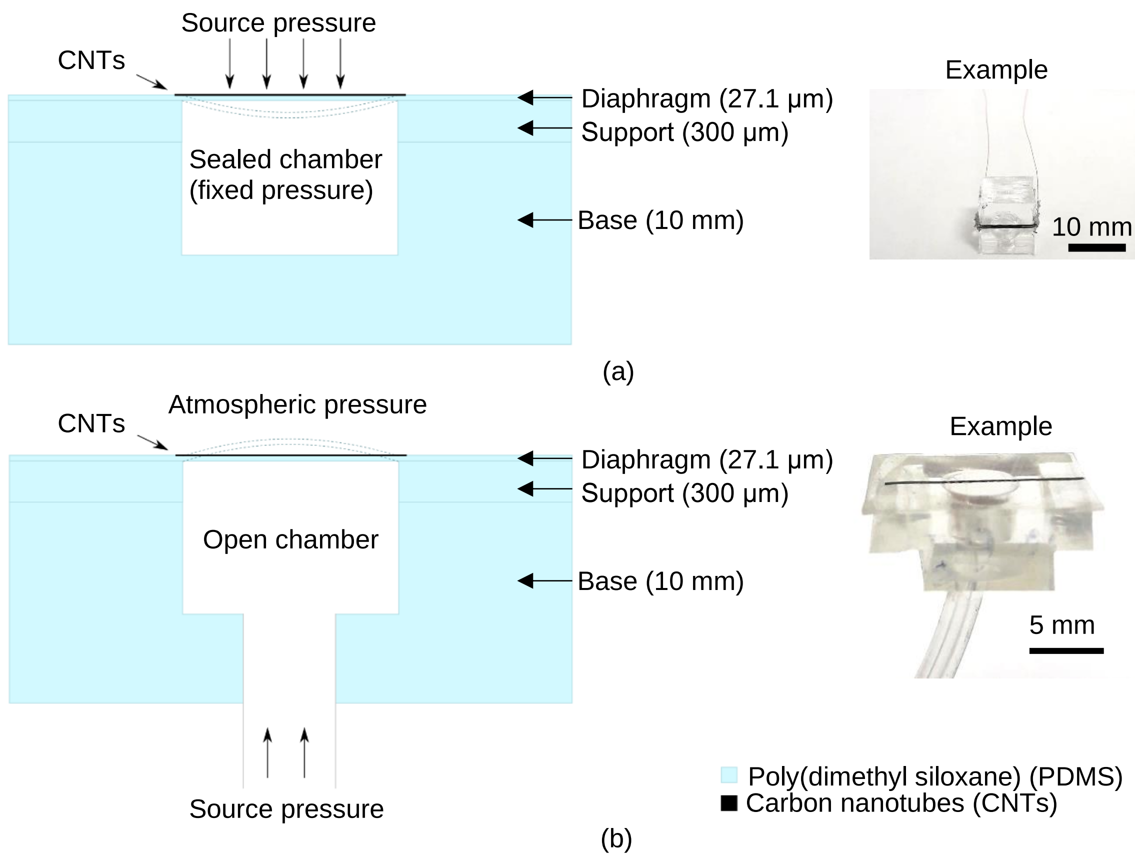

Figure 17. Schematic of the open chamber and sealed chamber configurations of pressure sensors: (a) in the sealed chamber configuration, the diaphragm and substrate form a sealed chamber, and (b) in the open chamber configuration a tube connected to the backside receives external pressure.

On the other hand, the gauge pressure sensor has a port that receives the source pressure, and its output is compared to atmospheric pressure (shown in Figure 17b). For the fabrication of the sealed gauge pressure sensor (sealed chamber), first, carbon nanotubes were inkjet-printed on PET film (Figure 18a). Then, PDMS was spin-coated on the PET film at several speeds to obtain diaphragms with varying degrees of thickness (Figure 18b). Previous studies have experimentally found that in the spin-coating procedure, as the spin speed increases, the thickness of the PDMS decreases [85]. The sample was then cured for one hour at 100 °C. In another layer of PDMS (300 µm), five millimeters (in diameter) holes were punched to define the chamber. This second layer was then bonded to the first layer to provide support for the diaphragm (Figure 18c). The bonding procedure consisted of applying corona discharge one centimeter away from both PDMS surfaces for one minute, then contacting both surfaces to be bonded and curing in an oven for one hour at 100 °C. In the following step, the PDMS was peeled off from the PET (Figure 18d). Since the thickness of the diaphragms in this study ranged from 90.8 µm to 27.1 µm, each sample was thermally treated to prevent tearing of the diaphragm, as described in section 3.3.6. The sample was then bonded to another block of PDMS that served as a structural element to form the chamber (Figure 18e), and finally, the electrical contacts were made with silver epoxy (Figure 18f).

For the fabrication of the gauge pressure sensor (open chamber), a similar procedure was used. However, in step (e) the top structure was peeled off from PET and bonded to a thick structure of PDMS that contained an opening on the front side and a tube connection on the backside. The resulting sensor had a PDMS diaphragm facing the front side (for atmospheric pressure) and a tube connection facing the backside (for variable source pressure), as shown in Figure 17b.

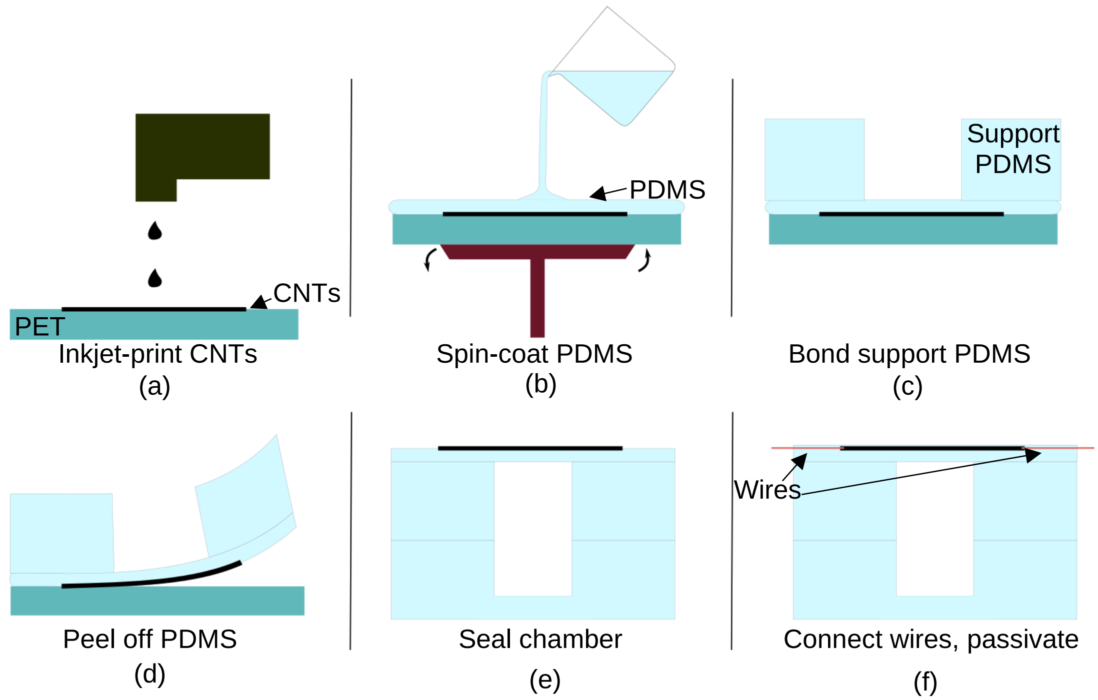

Figure 18. Fabrication steps of the pressure sensor: (a) carbon nanotubes were inkjet-printed on the PET film; (b) a thin PDMS membrane was spin-coated to form the diaphragm; (c) a support PDMS was bonded to the diaphragm; (d) the patterns were peeled off from PET; (e) the patterns were bonded to a thick PDMS to form the chamber, and (f) electrical connections were made with silver epoxy.

The fabrication procedure was optimized to fabricate reliable pressure sensors with low limit of detection. To achieve low limit of detection, one of the requirements was to obtain low diaphragm thickness. However, it was observed that if the thickness of the PDMS film was below 200 µm, the separation of PDMS from PET could not be performed successfully. Hence, a support PDMS layer was necessary to provide strength to the diaphragm during the peel off procedure. The support PDMS layer consisted of a film having a thickness of 300 µm and an opening with the desired diameter which was punched with a biopsy punching tool.

In addition to the support layer, another optimization was necessary since simply peeling off the diaphragm from PET sheet resulted in tearing of the diaphragm when the thickness was below

100 μm. Hence, a thermal treatment procedure was developed to reduce tearing of the diaphragm and to improve the yield of the produced diaphragms. The thermal treatment procedure is described in details in section 3.3.6.

One of the steps of the fabrication procedure is to bond the diaphragm to the PDMS chamber. It is known that corona discharge provides a reliable and permanent bond between PDMS layers [88]. In order to speed up the bonding after application of corona discharge, a curing procedure can be employed at elevated temperatures (100 °C). If the curing procedure is not employed, the permanent bonding takes longer (usually more than 24 hours). A curing procedure was employed by placing the PDMS into a pre-heated oven at 100 °C for one hour. However, it was observed that the diaphragm would become loose after removal from the oven. A loose diaphragm was detrimental to achieving a low limit of detection of the pressure sensors. Therefore, only the corona discharge treatment was employed for the permanent bonding of PDMS layers.

5.3. Experimental Setup

The experimental setup comprised a system containing the pressure sensor, a syringe, and a manometer. All of the components were connected through plastic (PTFE) tubing and sealed with silicone glue. The syringe was placed on a syringe pump (PHD 2000 from Harvard Apparatus, Holliston, MA). For actuation of the syringe, several actuation profiles were defined beforehand on the syringe pump. During measurement, the syringe pump automatically actuated the syringe based on the selected actuation profile.

The increase in pressure inside of the tubing system was controlled by the amount of syringe actuation. The syringe moved at constant speed, which resulted in the internal volume of the system to increase or decrease according to the direction of movement of the syringe. The diaphragm of the pressure sensor deflects whenever the internal pressure of the system changes. A decrease in volume inside the system caused an increase in pressure, according to Equation 3. Figure 19 shows the schematic of the experimental setup.

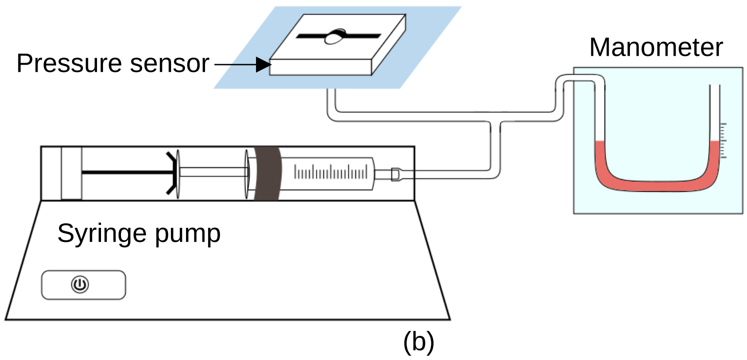

Figure 19. The experimental setup for measuring resistance change of the pressure sensor. The pressure was applied by a moving syringe in a closed system. When the volume of the closed system decreased, the pressure increased. A manometer was used to calibrate the output of the sensor to the applied pressure.

The manometer was employed to read the actual pressure inside of the tubing system and for later calibration of the resistance change to the pressure. The manometer is an instrument that measures the pressure difference between two ports. One port is connected to higher pressure, while the other port is connected to lower pressure (in this case, atmospheric pressure). The fluid inside the graduated scale moves according to the pressure difference between the ports. Although it is possible to measure pressure as low as 10 Pa, the manometer has some disadvantages: (1) due to the slow movement of the fluid, the manometer is not fast enough to detect rapid changes in pressure; and (2) it is an instrument that cannot be worn by a person since it is bulky and requires horizontal alignment. Nonetheless, the manometer is ideal for calibration of the pressure sensor at low pressure and slow pressure change. The full scale of the manometer was 700 Pa. In cases where the pressure applied was greater than the full scale of the manometer, the same was disconnected from the tubing and the ideal gas law was used to determine the pressure generated by a change in the volume of the system. The ideal gas law relates the pressure and volume of a gas in a closed system:

$$PV = nRT \tag{1}$$

where P is pressure, V is volume, n is the number of moles of gas in the system, R is the universal gas constant, and T is temperature.

The system does not gain or lose molecules (n stays constant) throughout the experiment, and the temperature of the system does not change (T stays constant). Boyle's law of gases states that in a closed system, the pressure increases when the volume decreases through the following relation:

$$P_i V_i = nRT = P_f V_f \tag{2}$$

where i indicates initial and f indicates final. If nRT is kept constant, the final pressure will be the initial pressure multiplied by the fractional volume change:

$$P_f = \frac{P_i V_i}{V_f} \tag{3}$$

The pressure difference ΔP is defined as the final pressure minus the initial pressure (ΔP is positive if the pressure increases):

$$\Delta P = P_f - P_i \tag{4}$$

The resistance was measured with a Keithley DMM 2110 multimeter. The reported percent resistance change was calculated from the difference in resistance ΔR, where $\Delta R = R - R_0$

(resistance minus the initial resistance):

$$Resistance\ change = \Delta R / R_0 \tag{5}$$

5.4. Working Mechanism of the Pressure Sensor Response

The pressure sensor can be described by two chambers which are separated by a diaphragm. If the pressure on the top chamber is higher than that on the bottom chamber, the diaphragm will deflect toward the bottom. The diaphragm is composed of a PDMS film which contains a patterned line of carbon nanotubes on its surface, so that when the diaphragm deflects, the length of the carbon nanotube line increases. The increase in length changes the resistance of the carbon nanotube line. The relative change in length of a material can be represented by the strain ε, which is defined as:

$$\varepsilon = \Delta L / L_0 \tag{6}$$

where ΔL is the change in length of the material and L_0 is the initial length.

5.5. Characterization of the Pressure Sensor

Pressure sensors were successfully fabricated and characterized in the low-pressure range from approximately 10 to 600 Pa, obtaining high sensitivity and low limit of detection. The use of the inkjet printer allowed direct deposition and patterning of carbon nanotubes onto the substrate film, with the subsequent transfer to PDMS. The pressure sensor is composed of a PDMS diaphragm that deflects when the gas pressure is higher on one side. The deflection generates a strain on the carbon nanotube line that is patterned in the center of the diaphragm. The pressure difference was calculated by measuring the resistance change due to the strain on the carbon nanotube line. In the following subsections, several performance characteristics of the pressure sensor are analyzed and discussed.

5.5.1. Diaphragm Thickness

Several aspects of the pressure sensor affect its response to a pressure change. Among them, the thickness of the diaphragm directly affects the amount of deflection due to an applied pressure. A thicker diaphragm offers more resistance to deflection. Hence, it is expected that a lower diaphragm thickness will produce a larger deflection, which translates to a higher sensitivity of the pressure sensor. Figure 20 shows the resistance change due to pressure changes for different diaphragm thicknesses.

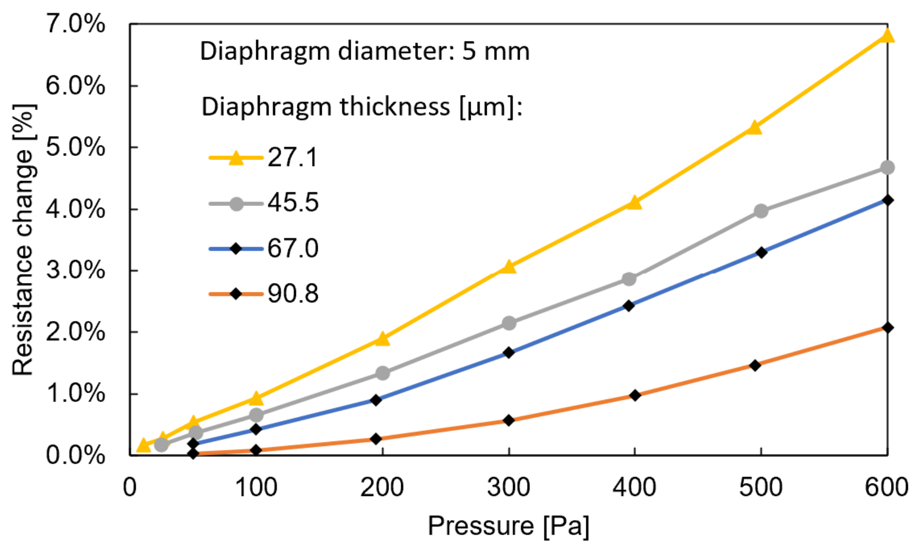

Figure 20. Response of the pressure sensor to different diaphragm thicknesses. All of the sensors had a diaphragm diameter of 5 mm, while the thicknesses studied ranged from 27.1 to 90.8 µm. Each data point represents the resistance change at a particular pressure applied to the sensor from the graph of Figure 21. The diaphragms with thicknesses of 67 and 90.8 µm did not show any resistance change when pressures below 100 Pa were applied. From this graph it is observed that lower diaphragm thickness generates a higher sensitivity.

Four pressure sensors were fabricated following the procedure described in section 5.2. Each diaphragm was formed by spinning the PDMS at a different speed, while the other conditions were kept equal. The thickness of the diaphragm depended on the spinning speed of the spin coating procedure. The speeds were 500, 700, 1000, and 1500 rpm, generating diaphragm thicknesses of 90.8, 67.0, 45.5, and 27.1 μm, respectively. In the range of thicknesses studied, increasing thickness corresponded to a lower resistance change for the same applied pressure. This result indicates that a lower diaphragm thickness is desirable to obtain a higher sensitivity of the pressure sensor. However, as described in chapter 3, the addition of a support PDMS layer and the application of a thermal treatment were both necessary for successfully peeling off the diaphragm, enabling diaphragms with thicknesses as low as 27.1 μm, which greatly enhanced the sensitivity of the pressure sensors. Table 4 summarizes the performance of the pressure sensors for the thicknesses studied.

Table 4. Summary of the thickness characterization of the pressure sensors.

Spin speed [rpm]	**Thickness [μm]**	**Sensitivity [%/kPa]**	**Limit of detection [Pa]**
500	90.8	3.66	5.5
700	67.0	7.28	3.1
1000	45.5	7.90	3.3
1500	27.1	10.99	3.1

5.5.2. Sensitivity

The sensitivity was analyzed for the previously fabricated pressure sensors. In each pressure sensor, an increasing pressure was applied to the sensor through actuation of the syringe. The pressure started at zero Pa, increased to 100 Pa, then decreased to zero Pa, followed by a thirty-seconds wait time. The next pressure was 200 Pa, and subsequently increasing until 600 Pa, as shown in Figure 21. A video recorder was used to record the actual pressure reading from the manometer. That is because the pressure was applied through the movement of the syringe and the actual pressure could be different than the nominal pressure. For example, if the nominal pressure is 100 Pa, the actual pressure might be 102 Pa.

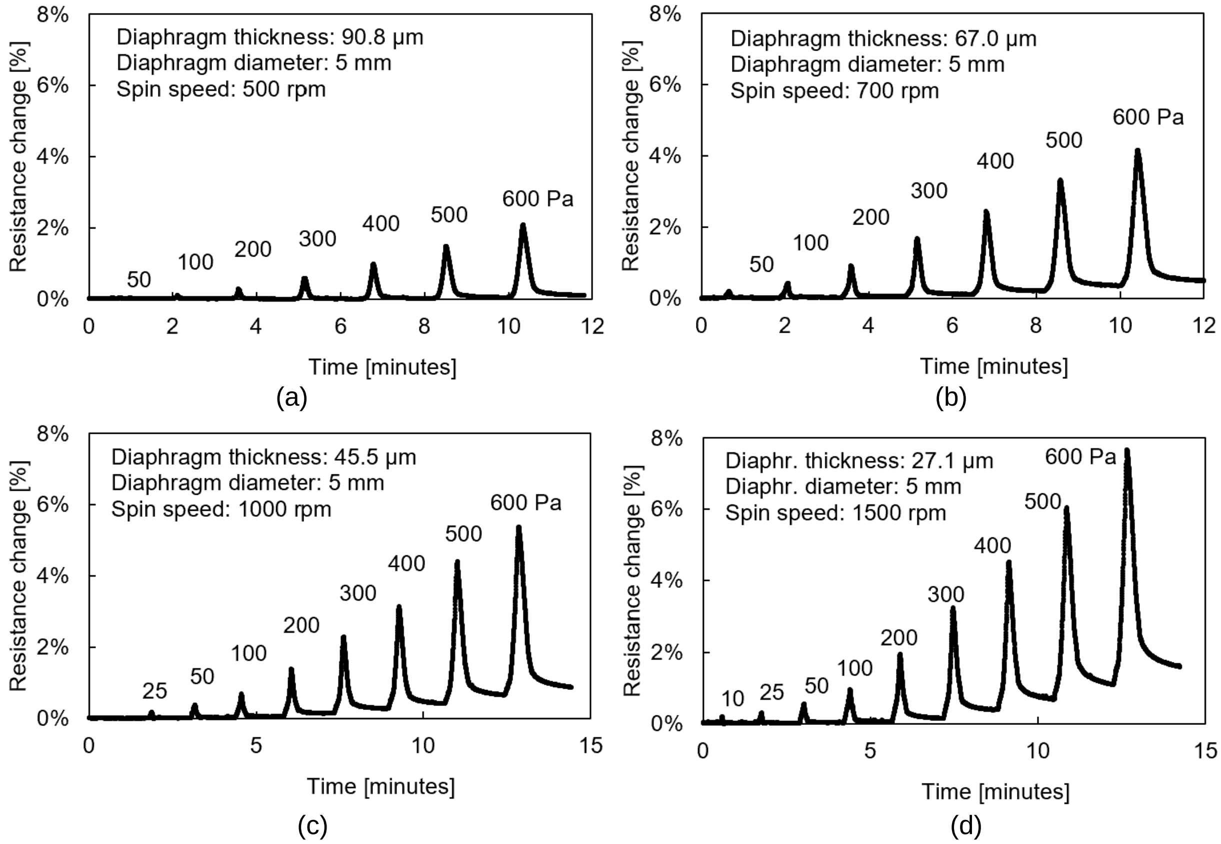

Figure 21. Sensitivity of pressure sensors for different diaphragm thicknesses: (a) sensitivity for diaphragm thickness of 90.8 μm was 3.66 %/kPa; (b) sensitivity for diaphragm thickness of 67.0 μm was 7.28 %/kPa; (c) sensitivity for diaphragm thickness of 45.5 μm was 7.90 %/kPa, and (d) sensitivity for diaphragm thickness of 27.1 μm was 10.99 %/kPa. All diaphragm diameters were 5 mm, while the thickness of the diaphragms varied. From the characterization of all the thicknesses, it was found that the sensitivity increases as the thickness decreases. In the range of thicknesses studied, the highest sensitivity was found to be for the thickness of 27.1 μm.

The resistance of the pressure sensor was measured with a Keithley 2110 multimeter and the peak value of the resistance at each pressure was recorded as the final resistance. The value before the application of each pressure was recorded for the initial resistance. The resistance change was then calculated as the final resistance minus the initial resistance, while the percent resistance change was calculated by dividing the resistance change by the initial resistance, according to Equation 5. For the sensitivity calculation, the slope of the calibration curve was obtained, and specified in %/kPa (percentage change in resistance per kilopascal).

5.5.3. Limit of Detection

The limit of detection is an important parameter that determines the minimum detectable pressure of the pressure sensors. The limit of detection was analyzed for the pressure sensors comprising different thicknesses. The setup shown in Figure 19 was used for the measurement of the minimum pressure. The manometer was connected between the syringe and the pressure sensor. For the repeated application of static pressure, the syringe moved by a fixed amount, raising the pressure to the specified value (shown on the manometer), then returning to the initial position. The pressure for the limit of detection was chosen based on the minimum detectable resistance change that was observed in the sensitivity plot of each sensor. For example, for the diaphragm with thickness of 90.8 µm, the chosen pressure was 100 Pa, which was the minimum pressure at which the change in resistance was discernible from noise, as seen in the sensitivity plot of Figure 21a. The applied pressure for the other thicknesses followed a similar reasoning. It is important to note that the diaphragm with the lowest thickness (27.1 µm) presented a discernible change in resistance when the pressure was only 10 Pa. As the thickness decreased, the pressure sensors presented a lower (improved) limit of detection. The graphs in Figure 22 demonstrate that the sensor can be applied in the detection of minute air pressure changes for a variety of applications in healthcare.

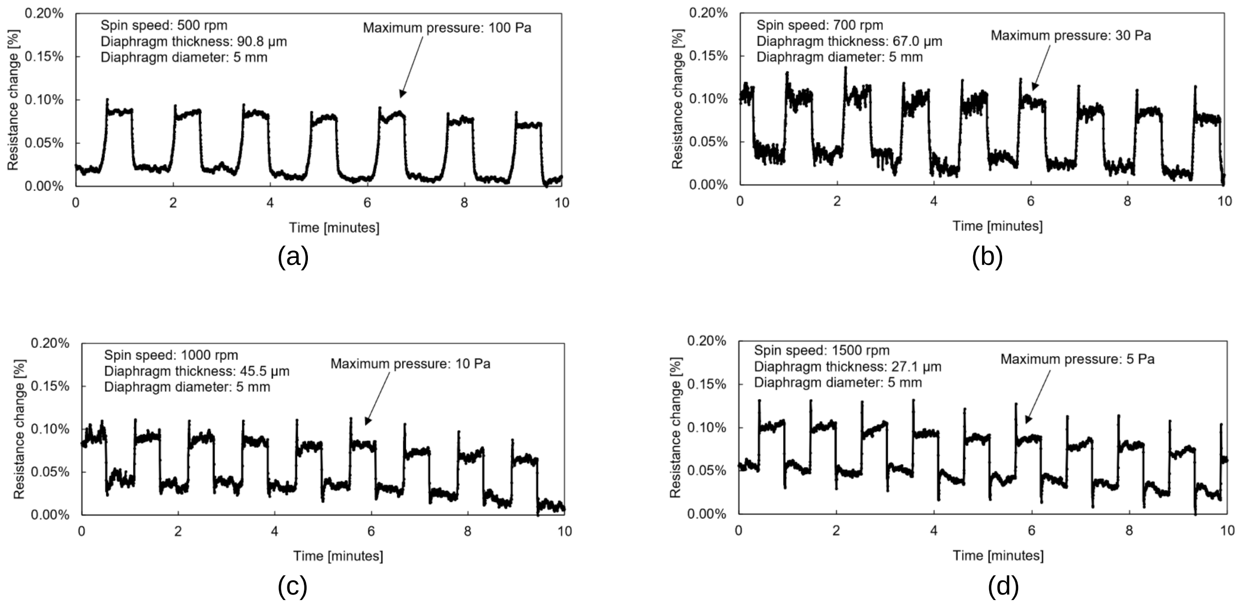

Figure 22. Limit of detection of pressure sensors with different diaphragm thicknesses. The limit of detection was 5.5, 3.1, 3.3, and 3.1 Pa for pressure sensors with thicknesses of 90.8, 67.0, 45.5, and 27.1 μm, respectively.

The limit of detection was calculated by following the steps given in [110]: first, pressure at or close to the expected limit of detection was applied to each sensor, then the average and the sample standard deviation s_y of eight samples were taken. Secondly, increasing pressures were applied to each sensor to obtain the calibration curve. With the data, the slope of the calibration curve r was obtained. The value of the student's t-function was used as $t = 3$. The limit of detection was then calculated as follows: $\chi_{LOD} = \frac{ts_y}{r}$.

The spikes in the change in resistance observed in the graphs of Figure 22 were caused by the manometer. Briefly, when the pressure changes and the fluid inside of the manometer moves, the fluid acquires a momentum. When the pressure suddenly stops increasing, the fluids keeps moving and the pressure inside the system suddenly decreases, thus generating the spike. This behavior was confirmed to happen only when the manometer was connected to the system.

When the manometer was disconnected, the spike did not happen.

The low limit of detection was achieved by reducing the noise level (by establishing stable electrical connections), and reducing the diaphragm thickness. The noise level directly affects the limit of detection, since the noise level is directly correlated to the sample standard deviation of the resistance readings. In addition to establishing stable electrical connections through silver epoxy, the copper wires were affixed to the measuring platform with tape so that minimal movement occurred during measurement. It has been observed that any wire movement caused noise in the measurement of the resistance. Lastly, the diaphragm thickness was reduced to allow a higher change in resistance at low pressures.

The implications of a low limit of detection are the possibility of using the sensor in applications where the pressure change is minimal, for example, in respiration monitoring. In addition, a signal with a higher quality is produced, since the signal contains less noise.

5.5.4. Pressure Speed

The response of the sensor was analyzed with respect to varying speeds in which the pressure changed. The pressure speed was defined as change in pressure per unit time (Pa/s). Figure 23 shows the resistance change due to pressure applied at different speeds. The graph shows that the amount of change in resistance does not significantly change for different speeds. In this experiment, the syringe moved at speeds of 0.5, 1.0, 1.5, 2.0, 2.5, and 3.0 ml/min. The pressure was not directly measured, since the manometer was disconnected. Instead, the pressure was calculated based on the amount of resistance change and the calibration plot. The difference between maximum and minimum response is 0.12%, which corresponds to a pressure well below 10 Pa. Therefore, the variation in resistance change is small compared to the applied pressure.

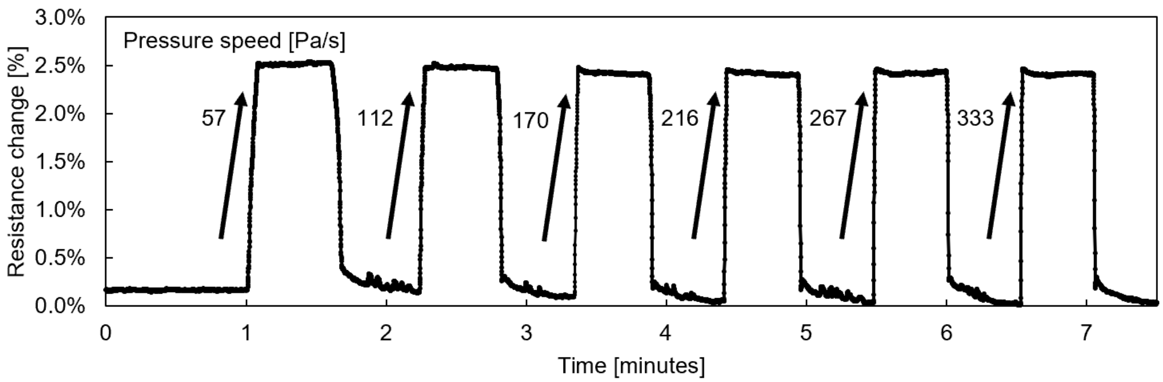

Figure 23. Characterization of the response of the sensor to different pressure speeds. The response did not significantly change when different speeds were applied. The difference in response was 0.12%, which is less than 10 Pa. The movement of the syringe was controlled to apply pressure at different speeds. The total pressure in each case was 250 Pa, and the pressure speed was calculated based on the total pressure and the time taken to reach the total pressure.

5.5.5. Repeatability

The repeatability of a single sensor was analyzed. The repeatability is reported in terms of the average of the error and the standard deviation of the error. The error is the difference between each measurement and the average of five measurements. Average of error is the average of five errors, while the standard deviation of the error is the sample standard deviation of five errors. The repeatability is usually reported in terms of full scale output, so in this case the full scale of the pressure sensor is 600 Pa. In this experiment, the pressure applied was 600 Pa (full scale) with a waiting time of five minutes between each pressure application. The data presented in Figure 24 was used to calculate the repeatability measures. The average change in resistance was 4.18% per 600 Pa of applied pressure, while the average of the error was 0.010% and the standard deviation of the error was 0.009%.

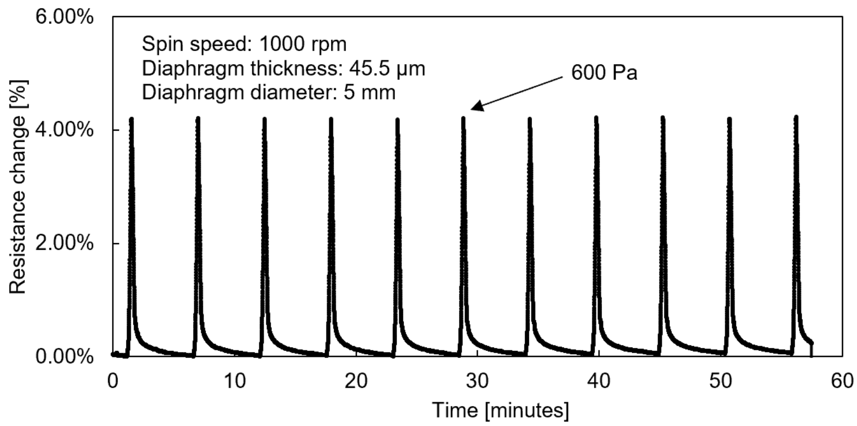

Figure 24. Repeatability of a single sensor. The average change in resistance was 4.18% per 600 Pa of applied pressure, while the average of the error was 0.010% and the standard deviation of the error was 0.009%.

5.5.6. Recovery Time

The recovery time of the pressure sensor was analyzed with respect to different maximum pressures applied. Figure 25 shows the recovery time for several pressures. In this experiment, a certain pressure was applied to the sensor in one second. Then, the pressure of the system was released while recording the resistance change of the pressure sensor. In all cases, the syringe was used to apply pressure to the system in one second. Different final pressures were obtained by moving the syringe at different speeds. The pressure applied at the end of one second were 10, 20, 40, 90, and 300 Pa. It is noted that the lowest recovery time occurs when the pressure is 10 Pa. When the applied pressure increases, so does the recovery time. For example, in the case of 90 Pa, the recovery time to reach 95% of the initial value is only 2.1 seconds. Figure 25 shows the recovery time for several pressures.

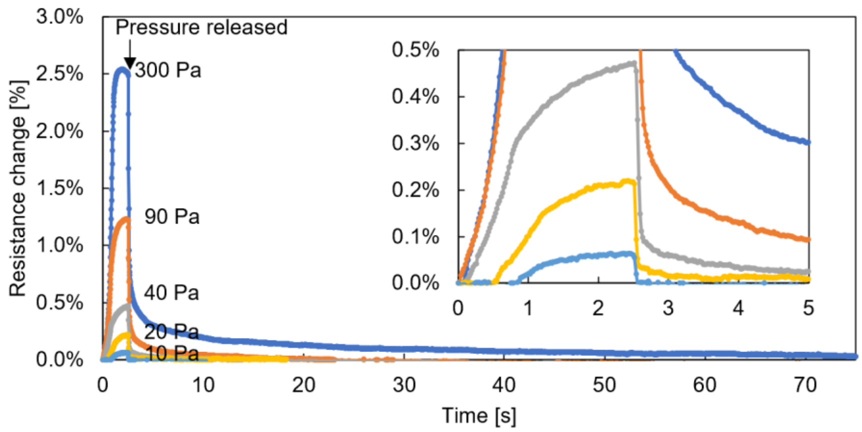

Figure 25. Recovery time of the pressure sensor for varying maximum pressure. When the applied pressure increases, so does the recovery time. In the case of 90 Pa, the recovery time to reach 95% of the initial value is only 2.1 seconds.

5.6. Discussion and Conclusions

The carbon nanotube line that crosses the PDMS diaphragm presents the behavior of resistance change when a strain is applied. When the PDMS membrane bulges outward due to deflection, the carbon nanotube pattern experiences a strain. However, the maximum strain will occur at the center of the diaphragm. If carbon nanotubes are patterned close to the edges, their strain will be much less at those places, and therefore, they do not contribute significantly to the overall resistance change. Because of this behavior, the line of carbon nanotubes crossing the center of the diaphragm provides an optimal resistance change.

It has been reported in the literature a range of structures that impart touch sensitivity to the pressure sensors. However, those structures are suboptimal because the thickness of the PDMS is always greater than the minimum obtainable, providing considerable rigidity. Thus the sensitivity obtained is in the range of a few percent change in resistance per kPa. The sensor structure based on diaphragm presents the minimum thickness achievable to the PDMS, offering higher sensitivity, namely a few percent change in resistance per Pa (compared to kPa). This sensitivity is a few orders of magnitude higher than those found in the literature.

Such low thickness of the diaphragm may raise the concern that air leakage could happen through the diaphragm. However, for the low pressure range of the order of tens of pascals, such low pressure is not enough to generate a significant leakage. In fact, an experiment was performed to measure any pressure drop due to leakage. The pressure sensor was connected to the manometer and the syringe through a plastic tubing, and the syringe was actuated so that the pressure measured by the manometer kept stable at two hundred pascals. During the experiment, which lasted for one hour, no pressure drop was observed on the manometer reading, indicating that the pressure sensor did not present any observable leakage in the period of one hour.

It should be mentioned that pressure sensors based on silicon diaphragms have achieved similar sensitivity to the one presented here [111]. However, limit of detection has not been reported in the literature for silicon-based pressure sensors [112]. Although silicon-based pressure sensors have their merits, the pressure sensors fabricated in this work do not require complex fabrication processes and make use of a class of polymer-based nanocomposite that may be employed in biocompatible sensors.

The extremely low limit of detection reported here has not been found in the literature for any other polymer-based pressure sensor [113]. Several factors have been taken into account during fabrication to allow such a low limit of detection. Among them, the reduction in diaphragm thickness was achieved by bonding a support PDMS layer to the diaphragm. Also, a thermal treatment was applied during the peeling off procedure, which allowed PDMS diaphragms with thicknesses down to 27.1 μm to be reliably peeled off. Further, a reduction in the noise level of the resistance was achieved by establishing stable electrical contacts between the carbon nanotubes and copper wires through silver epoxy.

CHAPTER 6. PRESSURE SENSOR APPLICATIONS

6.1. Pressure Generated by the Breathing Pattern

In the respiratory tract, airflow is driven by a pressure gradient [114]. During inhalation, negative pressure from the intrathoracic region is transmitted to the upper airway [115]. In other words, air flows into the lungs due to pressure differences between the alveolar pressure and ambient pressure. If the pressure inside the lungs is lower than that of the ambient, air flows in to fill the space (the reverse is also true). Therefore, it is conceivable that a pressure sensor sensitive enough will be able to detect those transient pressure differences. By recording and analyzing the pressure changes, it is possible to measure the respiratory rate as well as to detect abnormal breathing patterns. Several respiratory disorders can be identified with the detection of abnormal breathing patterns [116], including obstructive sleep apnea and pneumonia. In obstructive sleep apnea, the cyclic breathing pattern is disrupted by the cessation of airflow. Detection of those instances allows the identification and assessment of obstructive sleep apnea. For pneumonia, the respiratory rate of the patient is one of the measures used to identify the pneumonia severity index (PSI).

The pressure sensor with a closed chamber, as described in Figure 17a has many applications in healthcare, particularly in breathing monitoring. Some of the examples are respiration rate monitoring, breathing monitoring for pediatric care, and detection of sleep apnea events. The benefits of such a sensor include its biocompatibility and small form factor. The sensor proposed here is, therefore, well suited to measure the changes in pressure caused by breathing and, thus, provide detection of sleep apnea events.

6.2. Obstructive Sleep Apnea

Obstructive sleep apnea is a condition that affects millions of people worldwide. It is a disorder that prevents normal breathing due to repeated obstruction of the airway. Specifically, the muscles of the mouth relax during sleep, thus blocking the airways. Sleep apnea events can be detected because the person stops breathing; that is, there is a halt on the breathing pattern. Polysomnogram is the gold standard for the diagnosis of sleep apnea, but it is largely inconvenient. It requires that the person stays at the hospital overnight for measurement and recording of a variety of signals. In addition, real-time monitoring and detection of sleep apnea events by indirect measurements such as ECG are not satisfactory. Therefore, a simple approach that provides equivalent information will be beneficial for the identification and monitoring of obstructive sleep apnea events.

To detect air pressure changes when respiration stops, the sensor is placed inside the mouth, so that it measures the rhythmic pressure changes generated by normal respiration. When the upper airway relaxes, the airflow is blocked, and the pressure inside the mouth presents an erratic behavior (not changing for an extended period). By analyzing the pressure signal, the detection of when the person stops breathing becomes possible.

The sleep apnea pressure sensor provides a means of directly measuring pressure changes in the upper airway, and deviations from the cyclic breathing pattern can be detected for real-time monitoring. This type of sleep apnea assessment is more convenient for the patient to wear than polysomnogram and is more reliable than indirect methods.

6.2.1. Development of an Upper Airway Model

An upper airway model was developed to test the effectiveness of the pressure sensor in detecting pressure changes generated by breathing patterns. It is comprised of a 3D-printed structure containing a mouth, nose, and trachea (Figure 26a). A mechanical air pump generates the flow of air in a similar pattern to the flow found in an average person. Adults at rest have a respiration rate of about 20 breaths per minute, which means 20 inhalations and 20 exhalations within one minute. Hence, one inhalation lasts about 1.5 s, and one exhalation lasts another 1.5 s, resulting in the duration of one breathing cycle to be 3 s. In addition, the tidal volume of the lungs, that is, the volume of air exchanged in each breathing cycle is about 500 ml in adults. Therefore, a device that generates airflow was developed, capable of displacing 500 ml in 1.5 s to simulate both inhalations and exhalations. The 3D-printed model contained structures that follow the dimensions provided in the literature for average male adults. Specifically, the cross-sectional area of the trachea was found to be 194 mm^2 in women and 272 mm^2 in men [117] while the length was 100 mm [118]. Those values indicate that the diameter ranges between 15.7 mm and 18.6 mm. The nasal cavity dimensions are comprised of wedge-shaped spaces of approximately 50 mm in height and 50 mm in length. The cross-section of the nostrils is 5 mm x 10 mm, while the palatal height and width are 7.5 mm and 18.5 mm, respectively [119]. The 3D model contained an opening in the lower structure, which allowed the pressure sensor to be inserted into the 3D model, with the diaphragm facing the side from which air flows (Figure 26b). This is important for the detection of pressure differences through the Bernoulli effect.

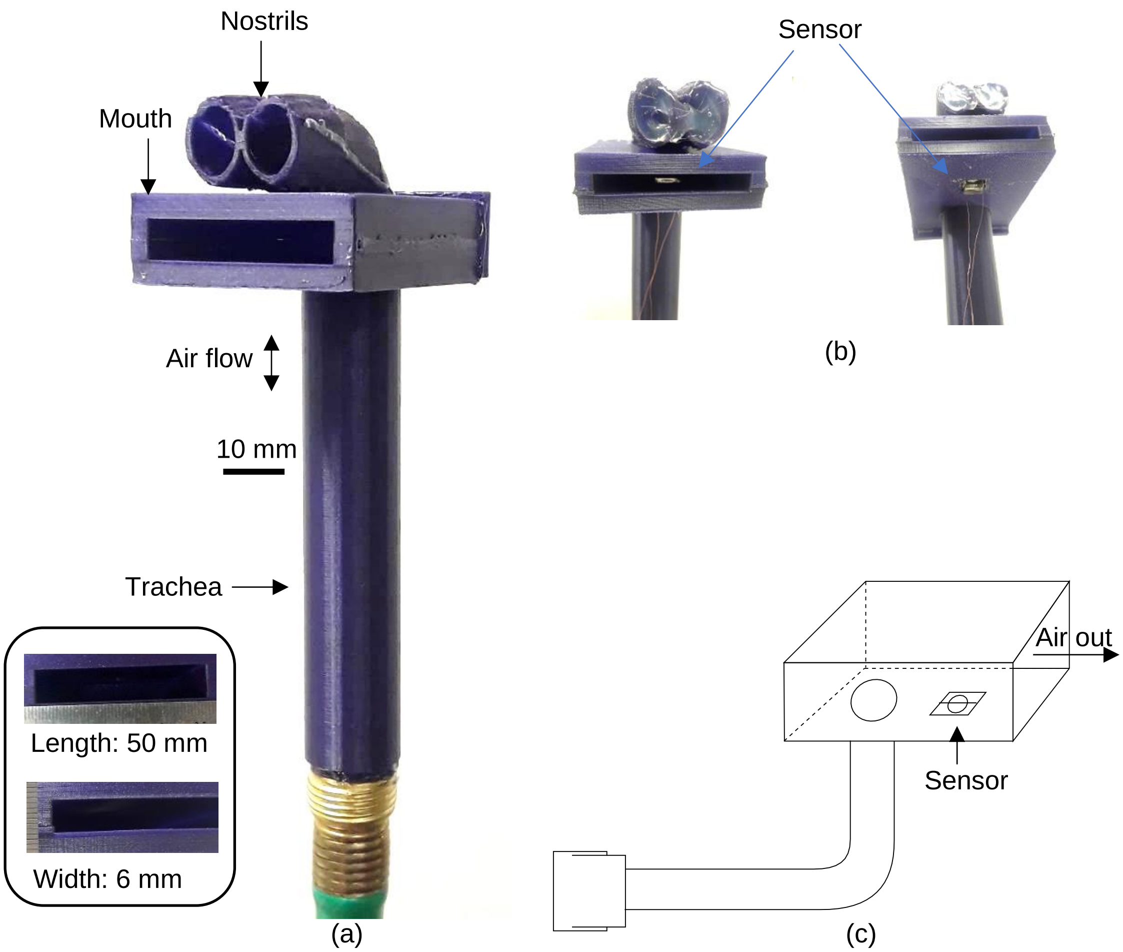

Figure 26. 3D-printed upper airway model: (a) picture of the complete 3D model. The model follows the dimensions of a person's upper airway system. It allows the sensor to be placed inside the mouth for testing breathing conditions; (b) pictures showing the placement of the sensor, and (c) schematic of airflow mechanism. The diameter of the diaphragm was five millimeters, and the thickness was twenty-seven micrometers.

The gauge pressure sensor (open chamber configuration) would not work to detect transient pressures such as those generated by breathing patterns since it requires a pressure source that is attached to the pressure port. For that reason, it is desirable to fabricate sealed gauge pressure sensors (closed chamber configuration). In this configuration, the sealed chamber contains a fixed pressure and volume, which are known at fabrication time. When pressure outside changes, the diaphragm expands/contracts accordingly.

6.2.2. Measurement of Pressure Changes Generated by Air Flow

In order to provide a characterization of the pressure sensor for potential use in human subjects, a mouth model was developed, which closely mimics the dimensions of an average person's upper airway system. The mouth model provides a flow of air, which decreases the pressure inside the model during airflow. By demonstrating that the sensor detects such low-pressure transients, it was possible to obtain pressure change information from the mouth model, which can be used to tune the parameters of the sensor for replication of the results in human subjects. Figure 27 shows the diagram of the airflow in the 3D model.

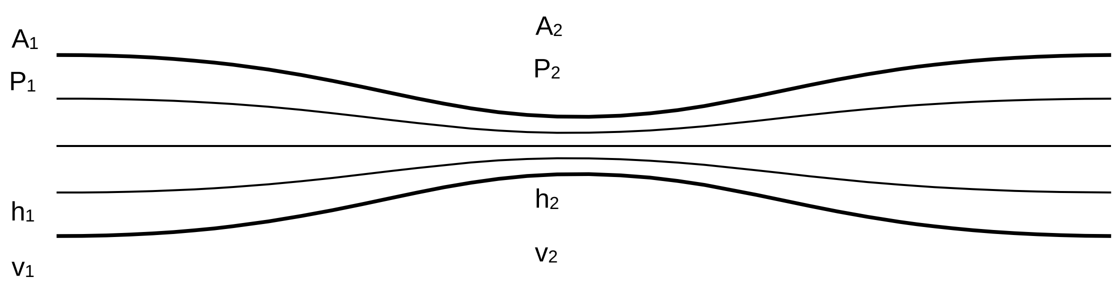

Figure 27. Schematic of airflow in the 3D model.

Referring to Figure 27, the pressure drop generated by fluid flow in a constriction can be described by the Bernoulli equation:

$$P_1 + \frac{1}{2}\rho v_1^2 + \rho g h_1 = P_2 + \frac{1}{2}\rho v_2^2 + \rho g h_2 \tag{7}$$

where P is pressure (Pa), ρ is volumetric density (kg/m^3), v is the velocity (m/s) along a streamline, h is the height (m), and g is the acceleration due to gravity (m/s^2). The numbers 1 and 2 indicate points along the same streamline. The formula assumes that the flow is steady and frictionless. If the effect of height is negligible ($h_1 - h_1 \approx 0$), the term containing height can be dropped. Solving for the pressure difference ($\Delta P = P_2 - P_1$), one obtains:

$$\Delta P = \frac{1}{2}\rho(v_1^2 - v_2^2) \tag{8}$$

The airflow rate Q is:

$$Q = \frac{V}{t} \tag{9}$$

where V is the volume (m^3), t is time (s), and Q is the volumetric flow rate (m^3/s).

The velocity of air v flowing through a cross-sectional area A is:

$$v = \frac{Q}{A} \tag{10}$$

where v is air velocity (m/s), Q is the volumetric flow rate (m^3/s), and A is cross-sectional area (m^2).

In the experiment using the 3D model, in each stroke of the airflow mechanism, 500 ml ($5*10^{-4}$ m^3) of air were displaced in 1 s, which gives an airflow rate Q of $5*10^{-4}$ m^3/s. The measured cross-sectional areas of point 1 and point 2 were 0.0095 m^2 and 0.003 m^2, respectively. From Equation 10, the air velocity v_1 is 0.053 m/s and v_2 is 1.67 m/s. The pressure difference ΔP is found by plugging in the values into Equation 8, giving ΔP as -1.7 Pa. This value represents a decrease in pressure at point 2 when there is airflow.

Figure 28 shows the resistance measurement of such a sensor when placed inside of the 3D mouth model. The simulated breathing cycles were generated by a mechanical ventilator that displaced 500 ml of air per cycle every ten seconds, then every five seconds. The diameter of the diaphragm was five millimeters, and the thickness of the diaphragm was twenty micrometers.

The diaphragm was obtained by spin-coating PDMS at the speed of 2200 rpm for 90 s. Figure 28 indicates that the sensor can detect the subtle pressure changes caused by airflow through the 3D mouth model.

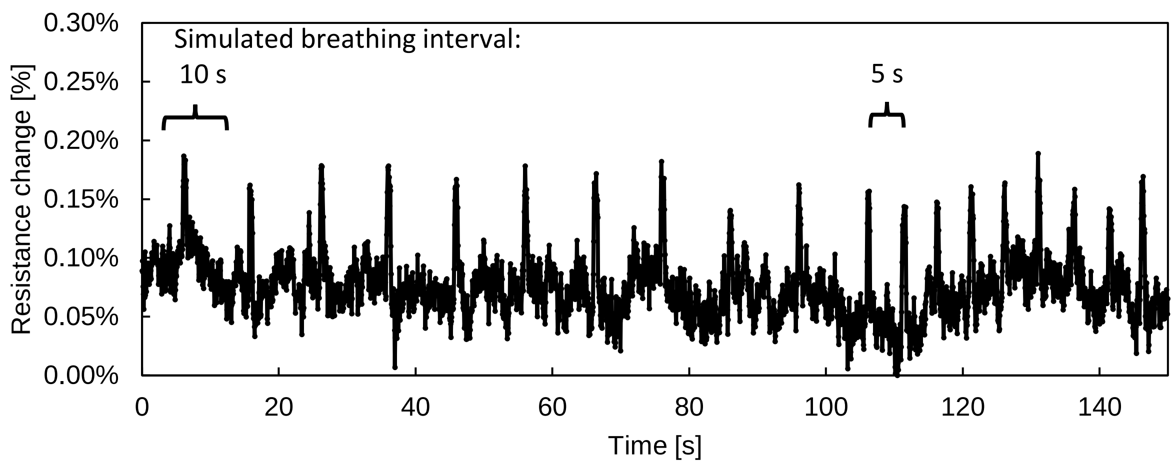

Figure 28. Resistance measurement corresponding to pressure changes generated by simulated breathing. The pressure sensor was positioned inside the 3D mouth model while the mechanical ventilation system provided airflow that simulated breathing cycles. The diameter of the diaphragm was five millimeters, and the thickness of the diaphragm was twenty micrometers.

6.3. Summary

In this chapter, pressure sensors capable of detecting minute air pressure changes were demonstrated as an application of the developed pressure sensor. The target application of the pressure sensor was the detection of sleep apnea events. In normal respiration, the cyclic breathing pattern causes pressure changes which are detected by the pressure sensor. When a sleep apnea event occurs, the missing air pressure changes provide information that the person has stopped breathing.

A 3D model was built to simulate the airflow passing through the human upper airway system. The 3D model contained a 3D mouth, nose, and trachea. In addition, the airflow was generated by a device that simulated the breathing of an average person. The pressure sensor was located inside of the 3D mouth model to acquire the cyclic breathing information. It was shown in the graph of Figure 28 the pressure changes caused by airflow at different breathing intervals.

CHAPTER 7. CONCLUSIONS AND FUTURE WORK

This chapter is devoted to conclude this work and to provide suggestions for future work.

7.1. Conclusions

7.1.1. Novel Transfer Printing Method for Patterning CNTs onto PDMS

Patterning of carbon nanotubes onto PDMS has been a challenge for the development of carbon nanotube/polymer composites. As a patterning method, inkjet printing is widely used to deposit inks of carbon nanomaterials onto different substrates. However, directly printing carbon nanotubes onto PDMS has been challenging mainly due to the coffee ring effect, which produces irregular patterns. In this dissertation, therefore, an alternative method was developed in which carbon nanotubes were first inkjet-printed onto PET film, then transferred to PDMS through transfer printing.

Although some organic solvents can help to disperse carbon nanotubes, aqueous inks are preferred since organic solvents might be toxic. In the ink formulation procedure, a comparison was performed between water and acetone solvents. It was found that a mixture of deionized water and sodium dodecyl sulfate (SDS) successfully disperses CNTs, whereas acetone does not disperse CNTs, even with the addition of SDS.

In the optimization of the transfer printing, the thermal treatment of the PET substrate played an important role in improving the transfer of CNTs to PDMS. At elevated temperatures, the PET becomes viscous, allowing the CNT/PDMS nanocomposite to be peeled off from PET with improved sheet resistance and higher yield.

With the method of transfer printing, uniformly deposited CNTs on PDMS were obtained, and two-dimensional force sensors were fabricated. The force sensors were composed of two layers of resistive sensing elements. When a force is applied perpendicularly to the film, the corresponding resistance increases, indicating the magnitude of the force as well as its position.

7.1.2. Development of Inkjet Printer for Deposition of Nanomaterials

Although inkjet printers are widely available at low cost, there is a limit on the achievable spatial resolution. Since multiple prints are required, and each print may add misalignment, the result is the lowering of spatial resolution. On the other hand, research-grade inkjet printers have a single or few nozzles with control of each droplet's position. However, those inkjet printers are expensive. Therefore, a custom inkjet printer was built that is low cost and provides high spatial resolution to the printed droplets. Characterization of the custom printer revealed that the minimum spacing between droplets was 18 μm, in which the limiting factor was the step of the motor. Finally, the minimum feature size of the printed pattern was determined by the diameter of a single printed droplet, which was measured as 120 μm.

7.1.3. Fabrication of Highly Sensitive Pressure Sensor

Using the transfer printing method developed in this work, highly sensitive pressure sensors were fabricated. The sensors operated in the low-pressure range (range from 10 Pa to 600 Pa), while the limit of detection was 3.1 Pa. In addition, it was shown that the sensitivity of the pressure sensor increased when the thickness of the diaphragm decreased. By changing the device parameters, the pressure sensor was optimized and achieved a better performance than polymer-based pressure sensors found in the literature, with the advantage of having a simple and low-cost fabrication. Moreover, the sensors can be employed in a variety of applications, such as monitoring of vital signals. As a demonstration of the measurement of pressure changes in the low-pressure range, the pressure sensor was placed inside a 3D-printed mouth model that was fabricated to simulate the breathing of an average person. Upon simulated airflow, the sensor detected minute pressure changes, thus confirming its ability to detect sleep apnea events.

7.2. Future Work

For future work, this research can be expanded and applied to other fields, which are described in the subsections below.

7.2.1. Integration of the Pressure Sensor in a Mouthpiece

To take advantage of the pressure sensor developed in this work in a clinical application, it is necessary a complete biomedical system that provides the auxiliary functions of energy storage, signal conditioning, and signal transmission. Those functions can be performed by a battery, microcontroller, and wireless transmission unit, respectively. Due to the extremely small size of electronic components, it is possible to condense all the required functions in a small form-factor printed circuit board that can be inserted into a mouthpiece. In addition to developing the auxiliary components, future work needs to reduce the size of the pressure sensor. Currently, the dimensions of the developed pressure sensor are 9 mm x 8 mm x 7 mm (length x width x height), which may prove difficult for seamless operation inside the mouthpiece. In addition, a sensing device in which the pressure sensor is part of a multiple-sensor system that includes pressure, temperature, and electrochemical sensors, would be beneficial for the systematic detection of other clinical conditions.

7.2.2. Multiple Sensor Array for Pressure Distribution Measurement

Tactile pressure sensors are increasingly being developed to measure the contact force applied to an area. In an extension of that concept, the single air pressure sensors described here can be manufactured on a common flexible and stretchable substrate to form an array of multiple pressure sensors. The consequent information from such a device is the pressure distribution of air on a surface. For instance, wind flowing around objects with complex geometry may be diverted, such that the air pressure distribution on the object's surface varies. In this modality of pressure measurement, the pressure being measured is the kinetic pressure which is due to air moving with a certain velocity. Depending on the velocity that the air hits the surface, more or less pressure is applied to that particular area. Therefore, a two-dimensional array of pressure sensors could identify the pressure distribution created by a particular airflow.

7.2.3. Optimization of Pressure Sensor Fabrication

In this work, efforts were focused on the development of a transfer printing process for carbon nanotubes (CNTs), with the aim to form a conductive film of CNTs on a flexible and stretchable polymer. Also, the applications of the conductive film were demonstrated through the fabrication and characterization of pressure sensors. Although the pressure sensors showed exceptional repeatability, the reproducibility among sensors needs to be improved. Several steps of the fabrication process are prone to small differences which affect the uniformity among the sensors and thus the reproducibility measure. For example, the application of the thermal treatment during the peeling off procedure currently relies on the manual adjustment of the distance between the hot air gun and the film, along with the time in which hot air is applied at each area of the film. Also, the actual temperature reached at the interface between PDMS and PET is currently not controllable, since only the nominal temperature of the hot air is controlled. Although the thermal treatment reduced the variability of the resistance and improved the yield of the peeled off diaphragms, controlling these parameters (distance, time, and temperature) would result in a higher reproducibility among sensors.

7.2.4. Extended Characterization of Pressure Sensor Parameters

For a pressure sensor that is composed simply of a diaphragm connecting two open chambers, such as the one characterized in Chapter 5, only the diaphragm offers a resistance to deflection. On the other hand, for a pressure sensor that is composed of a diaphragm and a sealed chamber, both the diaphragm and the compression of the air offer a resistance to deflection. Therefore, it is expected that a diaphragm assembled on a sealed chamber will show a lower sensitivity to pressure change, compared to a diaphragm assembled on an open (vented) chamber. Further studies on the quantitative effect of a sealed chamber should be performed to fully characterize the sealed gauge pressure sensor.

APPENDIX. PERMISSIONS

Permission for: T. H. da Costa and J.-W. Choi, “A flexible two dimensional force sensor using PDMS nanocomposite,” Microelectronic Engineering, vol. 174, pp. 64–69, 2017. doi: 10.1016/j.mee.2017.02.001.

A flexible two dimensional force sensor using PDMS nanocomposite

Author: Tallis H. da Costa,Jin-Woo Choi

Publication: Microelectronic Engineering

Publisher: Elsevier

Date: 25 April 2017

Please note that, as the author of this Elsevier article, you retain the right to include it in a thesis or dissertation, provided it is not published commercially. Permission is not required, but please ensure that you reference the journal as the original source. For more information on this and on your other retained rights, please visit: https://www.elsevier.com/about/our-business/policies/copyright#Author-rights

BACK CLOSE WINDOW

Permission for: T. H. da Costa and J.-W. Choi, “Low-cost and customizable inkjet printing for microelectrodes fabrication,” Micro and Nano Systems Letters, vol. 8, art. 2, 2020. doi: 10.1186/s40486-020-0104-7.

Publisher: Springer Nature

Creative Commons

This is an open access article distributed under the terms of the Creative Commons CC BY license, which permits unrestricted use, distribution, and reproduction in any medium, provided the original work is properly cited.

You are not required to obtain permission to reuse this article.

To request permission for a type of use not listed, please contact Springer Nature

Permission for: T. H. da Costa and J.-W. Choi, “Fabrication and Patterning Methods of Flexible

Sensors Using Carbon Nanomaterials on Polymers," Advanced Intelligent Systems, vol. 2, art. 1900179, 2020. doi: 10.1002/aisy.201900179.

REFERENCES

[1] W. D. Pilkey, “Microelectromechanical systems (MEMS),” in *Formulas for Stress, Strain, and Structural Matrices*, 2nd ed., Hoboken, NJ, USA: John Wiley & Sons, 2005, pp. 184–185.

[2] DuPont, “DuPont™ Kapton® summary of properties,” DuPont. https://www.dupont.com (accessed: Feb. 17, 2020).

[3] F. M. Sciammarella, C. A. Sciammarella, L. Lamberti, M. Styrcula, L. Wei, and A. Lakhtakia, “Robust mechanical property measurements of fibrous parylene-C thin-film substrate via moiré contouring technology,” *Journal of the Mechanical Behavior of Biomedical Materials*, vol. 20, pp. 237–248, Apr. 2013.

[4] I. D. Johnston, D. K. McCluskey, C. K. L. Tan, and M. C. Tracey, “Mechanical characterization of bulk Sylgard 184 for microfluidics and microengineering,” *Journal of Micromechanics and Microengineering*, vol. 24, no. 3, Art. no. 035017 (7pp), Mar. 2014.

[5] S. C. B. Mannsfeld, B. C.-K. Tee, R. M. Stoltenberg, C. V. H.-H. Chen, S. Barman, B. V. O. Muir, A. N. Sokolov, C. Reese, and Z. Bao, “Highly sensitive flexible pressure sensors with microstructured rubber dielectric layers,” *Nature Materials*, vol. 9, no. 10, pp. 859–864, Oct. 2010.

[6] J. Park, Y. Lee, J. Hong, M. Ha, Y.-D. Jung, H. Lim, S. Y. Kim, and H. Ko, “Giant tunneling piezoresistance of composite elastomers with interlocked microdome arrays for ultrasensitive and multimodal electronic skins,” *ACS Nano*, vol. 8, no. 5, pp. 4689–4697, May 2014.

[7] K.-H. Kim, S. K. Hong, N.-S. Jang, S.-H. Ha, H. W. Lee, and J.-M. Kim, “Wearable resistive pressure sensor based on highly flexible carbon composite conductors with irregular surface morphology,” *ACS Applied Materials & Interfaces*, vol. 9, no. 20, pp. 17499–17507, May 2017.

[8] B. Su, S. Gong, Z. Ma, L. W. Yap, and W. Cheng, “Mimosa-inspired design of a flexible pressure sensor with touch sensitivity,” *Small*, vol. 11, no. 16, pp. 1886–1891, Apr. 2015.

[9] Y. Yang and W. Gao, “Wearable and flexible electronics for continuous molecular monitoring,” *Chemical Society Reviews*, vol. 48, no. 6, pp. 1465–1491, Mar. 2019.

[10] J. Kim, A. S. Campbell, and J. Wang, “Wearable non-invasive epidermal glucose sensors: a review,” *Talanta*, vol. 177, pp. 163–170, Jan. 2018.

[11] A. Martín, J. Kim, J. F. Kurniawan, J. R. Sempionatto, J. R. Moreto, G. Tang, A. S. Campbell, A. Shin, M. Y. Lee, X. Liu, and J. Wang, “Epidermal microfluidic electrochemical detection system: enhanced sweat sampling and metabolite detection,” *ACS Sensors*, vol. 2, no. 12, pp. 1860–1868, Dec. 2017.

[12] Q. Wang, M. Jian, C. Wang, and Y. Zhang, “Carbonized silk nanofiber membrane for

transparent and sensitive electronic skin," *Advanced Functional Materials*, vol. 27, no. 9, Art. no. 1605657 (9pp), Mar. 2017.

[13] I. Kim, K. Woo, Z. Zhong, P. Ko, Y. Jang, M. Jung, J. Jo, S. Kwon, S.-H. Lee, S. Lee, H. Youn, and J. Moon, "A photonic sintering derived Ag flake/nanoparticle-based highly sensitive stretchable strain sensor for human motion monitoring," *Nanoscale*, vol. 10, no. 17, pp. 7890–7897, May 2018.

[14] S.-J. Choi, H. Yu, J.-S. Jang, M.-H. Kim, S.-J. Kim, H. S. Jeong, and I.-D. Kim, "Nitrogen-doped single graphene fiber with platinum water dissociation catalyst for wearable humidity sensor," *Small*, vol. 14, no. 13, Art. no. 1703934 (9pp), Mar. 2018.

[15] Y. Wei, Y. Qiao, G. Jiang, Y. Wang, F. Wang, M. Li, Y. Zhao, Y. Tian, G. Gou, S. Tan, H. Tian, Y. Yang, and T.-L. Ren, "A wearable skinlike ultra-sensitive artificial graphene throat," *ACS Nano*, vol. 13, no. 8, pp. 8639–8647, Aug. 2019.

[16] Q.-J. Sun, X.-H. Zhao, Y. Zhou, C.-C. Yeung, W. Wu, S. Venkatesh, Z.-X. Xu, J. J. Wylie, W.-J. Li, and V. A. L. Roy, "Fingertip-skin-inspired highly sensitive and multifunctional sensor with hierarchically structured conductive graphite/polydimethylsiloxane foams," *Advanced Functional Materials*, vol. 29, no. 18, Art. no. 1808829 (11pp), May 2019.

[17] B. Yin, X. Liu, H. Gao, T. Fu, and J. Yao, "Bioinspired and bristled microparticles for ultrasensitive pressure and strain sensors," *Nature Communications*, vol. 9, no. 1, Art. no. 5161 (8pp), Dec. 2018.

[18] S. Lin, B. Wang, Y. Zhao, R. Shih, X. Cheng, W. Yu, H. Hojaiji, H. Lin, C. Hoffman, D. Ly, J. Tan, Y. Chen, D. Di Carlo, C. Milla, and S. Emaminejad, "Natural perspiration sampling and in situ electrochemical analysis with hydrogel micropatches for user-identifiable and wireless chemo/biosensing," *ACS Sensors*, vol. 5, no. 1, pp. 93–102, Jan. 2020.

[19] T. Q. Trung, T. M. L. Dang, S. Ramasundaram, P. T. Toi, S. Y. Park, and N.-E. Lee, "A stretchable strain-insensitive temperature sensor based on free-standing elastomeric composite fibers for on-body monitoring of skin temperature," *ACS Applied Materials & Interfaces*, vol. 11, no. 2, pp. 2317–2327, Jan. 2019.

[20] D. Tasis, N. Tagmatarchis, A. Bianco, and M. Prato, "Chemistry of carbon nanotubes," *Chemical Reviews*, vol. 106, no. 3, pp. 1105–1136, Mar. 2006.

[21] A. Kamyshny and S. Magdassi, "Conductive nanomaterials for printed electronics," *Small*, vol. 10, no. 17, pp. 3515–3535, Sep. 2014.

[22] D. S. Hecht, L. Hu, and G. Irvin, "Emerging transparent electrodes based on thin films of carbon nanotubes, graphene, and metallic nanostructures," *Advanced Materials*, vol. 23, no. 13, pp. 1482–1513, Apr. 2011.

[23] J. P. Lu and J. Han, "Carbon nanotubes and nanotube-based nano devices," *International*

Journal of High Speed Electronics and Systems, vol. 09, no. 01, pp. 101–123, 1998.

[24] X. Zang, Q. Zhou, J. Chang, Y. Liu, and L. Lin, “Graphene and carbon nanotube (CNT) in MEMS/NEMS applications,” *Microelectronic Engineering*, vol. 132, pp. 192–206, Jan. 2015.

[25] A. Chen and S. Chatterjee, “Nanomaterials based electrochemical sensors for biomedical applications,” *Chemical Society Reviews*, vol. 42, no. 12, pp. 5425–5438, Jun. 2013.

[26] M. Trojanowicz, “Analytical applications of carbon nanotubes: a review,” *TrAC Trends in Analytical Chemistry*, vol. 25, no. 5, pp. 480–489, May 2006.

[27] H. Y. Mao, S. Laurent, W. Chen, O. Akhavan, M. Imani, A. A. Ashkarran, and M. Mahmoudi, “Graphene: promises, facts, opportunities, and challenges in nanomedicine,” *Chemical Reviews*, vol. 113, no. 5, pp. 3407–3424, May 2013.

[28] K. P. Loh, Q. Bao, P. K. Ang, and J. Yang, “The chemistry of graphene,” *Journal of Materials Chemistry*, vol. 20, no. 12, pp. 2277–2289, 2010.

[29] J. Du, S. Pei, L. Ma, and H.-M. Cheng, “25th anniversary article: carbon nanotube- and graphene-based transparent conductive films for optoelectronic devices,” *Advanced Materials*, vol. 26, no. 13, pp. 1958–1991, Apr. 2014.

[30] A. Carlson, A. M. Bowen, Y. Huang, R. G. Nuzzo, and J. A. Rogers, “Transfer printing techniques for materials assembly and micro/nanodevice fabrication,” *Advanced Materials*, vol. 24, no. 39, pp. 5284–5318, Oct. 2012.

[31] C. Park, Z. Ounaies, K. A. Watson, R. E. Crooks, J. S. Jr, S. E. Lowther, J. W. Connell, E. J. Siochi, J. S. Harrison, and T. L. S. Clair, “Dispersion of single wall carbon nanotubes by in situ polymerization under sonication,” *Chemical Physics Letters*, vol. 364, no. 3–4, pp. 303–308, Oct. 2002.

[32] J. Hwang, J. Jang, K. Hong, K. N. Kim, J. H. Han, K. Shin, and C. E. Park, “Poly(3-hexylthiophene) wrapped carbon nanotube/poly(dimethylsiloxane) composites for use in finger-sensing piezoresistive pressure sensors,” *Carbon*, vol. 49, no. 1, pp. 106–110, Jan. 2011.

[33] C. H. Liu, H. Huang, Y. Wu, and S. S. Fan, “Thermal conductivity improvement of silicone elastomer with carbon nanotube loading,” *Applied Physics Letters*, vol. 84, no. 21, pp. 4248–4250, May 2004.

[34] T. Sekitani, H. Nakajima, H. Maeda, T. Fukushima, T. Aida, K. Hata, and T. Someya, “Stretchable active-matrix organic light-emitting diode display using printable elastic conductors,” *Nature Materials*, vol. 8, no. 6, pp. 494–499, Jun. 2009.

[35] S. De, P. E. Lyons, S. Sorel, E. M. Doherty, P. J. King, W. J. Blau, P. N. Nirmalraj, J. J. Boland, V. Scardaci, J. Joimel, and J. N. Coleman, “Transparent, flexible, and highly conductive thin films based on polymer−nanotube composites,” *ACS Nano*, vol. 3, no. 3,

pp. 714–720, Mar. 2009.

[36] X. Song, S. Liu, Z. Gan, Q. Lv, H. Cao, and H. Yan, "Controllable fabrication of carbon nanotube-polymer hybrid thin film for strain sensing," *Microelectronic Engineering*, vol. 86, no. 11, pp. 2330–2333, Nov. 2009.

[37] Q. Cao, S.-H. Hur, Z.-T. Zhu, Y. G. Sun, C.-J. Wang, M. A. Meitl, M. Shim, and J. A. Rogers, "Highly bendable, transparent thin-film transistors that use carbon-nanotube-based conductors and semiconductors with elastomeric dielectrics," *Advanced Materials*, vol. 18, no. 3, pp. 304–309, Feb. 2006.

[38] D. Kim, D. Jung, J. H. Yoo, Y. Lee, W. Choi, G. S. Lee, K. Yoo, and J.-B. Lee, "Stretchable and bendable carbon nanotube on PDMS super-lyophobic sheet for liquid metal manipulation," *Journal of Micromechanics and Microengineering*, vol. 24, no. 5, Art. no. 055018 (6pp), May 2014.

[39] C.-X. Liu and J.-W. Choi, "Patterning conductive PDMS nanocomposite in an elastomer using microcontact printing," *Journal of Micromechanics and Microengineering*, vol. 19, no. 8, Art. no. 085019 (7pp), Aug. 2009.

[40] D. J. Lipomi, M. Vosgueritchian, B. C.-K. Tee, S. L. Hellstrom, J. A. Lee, C. H. Fox, and Z. Bao, "Skin-like pressure and strain sensors based on transparent elastic films of carbon nanotubes," *Nature Nanotechnology*, vol. 6, no. 12, pp. 788–792, Dec. 2011.

[41] M. Brun, J.-F. Chateaux, A.-L. Deman, P. Pittet, and R. Ferrigno, "Nanocomposite carbon-PDMS material for chip-based electrochemical detection," *Electroanalysis*, vol. 23, no. 2, pp. 321–324, Feb. 2011.

[42] A. Charalambides and S. Bergbreiter, "Rapid manufacturing of mechanoreceptive skins for slip detection in robotic grasping," *Advanced Materials Technologies*, vol. 2, no. 1, Art. no. 1600188 (10pp), Jan. 2017.

[43] M. Kujawski, J. D. Pearse, and E. Smela, "Elastomers filled with exfoliated graphite as compliant electrodes," *Carbon*, vol. 48, no. 9, pp. 2409–2417, Aug. 2010.

[44] T. H. da Costa and J.-W. Choi, "A flexible two dimensional force sensor using PDMS nanocomposite," *Microelectronic Engineering*, vol. 174, pp. 64–69, Apr. 2017.

[45] W. J. Xu, M. Kranz, S. H. Kim, and M. G. Allen, "Micropatternable elastic electrets based on a PDMS/carbon nanotube composite," *Journal of Micromechanics and Microengineering*, vol. 20, no. 10, Art. no. 104003 (7pp), Oct. 2010.

[46] J. Wu, Y.-M. Sun, Z. Wu, X. Li, N. Wang, K. Tao, and G. P. Wang, "Carbon nanocoil-based fast-response and flexible humidity sensor for multifunctional applications," *ACS Applied Materials & Interfaces*, vol. 11, no. 4, pp. 4242–4251, Jan. 2019.

[47] X. He, W. Gao, L. Xie, B. Li, Q. Zhang, S. Lei, J. M. Robinson, E. H. Hároz, S. K. Doorn, W. Wang, R. Vajtai, P. M. Ajayan, W. W. Adams, R. H. Hauge, and J. Kono, "Wafer-

scale monodomain films of spontaneously aligned single-walled carbon nanotubes," *Nature Nanotechnology*, vol. 11, no. 7, pp. 633–638, Jul. 2016.

[48] D. Zhang, K. Ryu, X. Liu, E. Polikarpov, J. Ly, M. E. Tompson, and C. Zhou, "Transparent, conductive, and flexible carbon nanotube films and their application in organic light-emitting diodes," *Nano Letters*, vol. 6, no. 9, pp. 1880–1886, Sep. 2006.

[49] C. Lim, D.-H. Min, and S.-B. Lee, "Direct patterning of carbon nanotube network devices by selective vacuum filtration," *Applied Physics Letters*, vol. 91, no. 24, Art. no. 243117 (3pp), Dec. 2007.

[50] Y. Zhou, L. Hu, and G. Grüner, "A method of printing carbon nanotube thin films," *Applied Physics Letters*, vol. 88, no. 12, Art. no. 123109 (3pp), Mar. 2006.

[51] L. Hu, G. Gruner, D. Li, R. B. Kaner, and J. Cech, "Patternable transparent carbon nanotube films for electrochromic devices," *Journal of Applied Physics*, vol. 101, no. 1, Art. no. 016102 (3pp), Jan. 2007.

[52] K. Lee, S. S. Lee, J. A. Lee, K.-C. Lee, and S. Ji, "Carbon nanotube film piezoresistors embedded in polymer membranes," *Applied Physics Letters*, vol. 96, no. 1, Art. no. 013511 (3pp), Jan. 2010.

[53] M. A. Meitl, Y. Zhou, A. Gaur, S. Jeon, M. L. Usrey, M. S. Strano, and J. A. Rogers, "Solution casting and transfer printing single-walled carbon nanotube films," *Nano Letters*, vol. 4, no. 9, pp. 1643–1647, Sep. 2004.

[54] S. Alom Ruiz and C. S. Chen, "Microcontact printing: a tool to pattern," *Soft Matter*, vol. 3, no. 2, pp. 168–177, 2007.

[55] Q. Bu, Y. Zhan, F. He, M. Lavorgna, and H. Xia, "Stretchable conductive films based on carbon nanomaterials prepared by spray coating," *Journal of Applied Polymer Science*, vol. 133, no. 15, Art. no. 43243 (8pp), Apr. 2016.

[56] D. Kim and K.-S. Yun, "Patterning of carbon nanotube films on PDMS using SU-8 microstructures," *Microsystem Technologies*, vol. 19, no. 5, pp. 743–748, May 2013.

[57] C.-X. Liu and J.-W. Choi, "Improved dispersion of carbon nanotubes in polymers at high concentrations," *Nanomaterials*, vol. 2, no. 4, pp. 329–347, Oct. 2012.

[58] S. Noimark, R. J. Colchester, B. J. Blackburn, E. Z. Zhang, E. J. Alles, S. Ourselin, P. C. Beard, I. Papakonstantinou, I. P. Parkin, and A. E. Desjardins, "Carbon-nanotube-PDMS composite coatings on optical fibers for all-optical ultrasound imaging," *Advanced Functional Materials*, vol. 26, no. 46, pp. 8390–8396, Dec. 2016.

[59] C. Lee, L. Jug, and E. Meng, "High strain biocompatible polydimethylsiloxane-based conductive graphene and multiwalled carbon nanotube nanocomposite strain sensors," *Applied Physics Letters*, vol. 102, no. 18, Art. no. 183511 (5pp), May 2013.

[60] C. Phillips, A. Al-Ahmadi, S.-J. Potts, T. Claypole, and D. Deganello, "The effect of graphite and carbon black ratios on conductive ink performance," *Journal of Materials Science*, vol. 52, no. 16, pp. 9520–9530, Aug. 2017.

[61] Y. Liao, R. Zhang, H. Wang, S. Ye, Y. Zhou, T. Ma, J. Zhu, L. D. Pfefferle, and J. Qian, "Highly conductive carbon-based aqueous inks toward electroluminescent devices, printed capacitive sensors and flexible wearable electronics," *RSC Advances*, vol. 9, no. 27, pp. 15184–15189, 2019.

[62] Y. Aleeva and B. Pignataro, "Recent advances in upscalable wet methods and ink formulations for printed electronics," *Journal of Materials Chemistry C*, vol. 2, no. 32, pp. 6436–6453, Aug. 2014.

[63] F. Sajed and C. Rutherglen, "All-printed and transparent single walled carbon nanotube thin film transistor devices," *Applied Physics Letters*, vol. 103, no. 14, Art. no. 143303 (4pp), Sep. 2013.

[64] A. Salim and S. Lim, "Review of recent inkjet-printed capacitive tactile sensors," *Sensors*, vol. 17, no. 11, Art. no. 2593 (20pp), Nov. 2017.

[65] L. Gonzalez-Macia, A. Morrin, M. R. Smyth, and A. J. Killard, "Advanced printing and deposition methodologies for the fabrication of biosensors and biodevices," *Analyst*, vol. 135, no. 5, pp. 845–867, 2010.

[66] R. Tortorich and J.-W. Choi, "Inkjet printing of carbon nanotubes," *Nanomaterials*, vol. 3, no. 3, pp. 453–468, Sep. 2013.

[67] J. M. Hoey, A. Lutfurakhmanov, D. L. Schulz, and I. S. Akhatov, "A review on aerosol-based direct-write and its applications for microelectronics," *Journal of Nanotechnology*, vol. 2012/09/05, Art. no. 324380 (22pp), 2012.

[68] K. J. Loh, J. P. Lynch, B. S. Shim, and N. A. Kotov, "Tailoring piezoresistive sensitivity of multilayer carbon nanotube composite strain sensors," *Journal of Intelligent Material Systems and Structures*, vol. 19, no. 7, pp. 747–764, Jul. 2008.

[69] D. Qian, E. C. Dickey, R. Andrews, and T. Rantell, "Load transfer and deformation mechanisms in carbon nanotube-polystyrene composites," *Applied Physics Letters*, vol. 76, no. 20, pp. 2868–2870, May 2000.

[70] M. H. Andrew Ng, L. T. Hartadi, H. Tan, and C. H. Patrick Poa, "Efficient coating of transparent and conductive carbon nanotube thin films on plastic substrates," *Nanotechnology*, vol. 19, no. 20, Art. no. 205703 (5pp), May 2008.

[71] N. Saran, K. Parikh, D.-S. Suh, E. Muñoz, H. Kolla, and S. K. Manohar, "Fabrication and characterization of thin films of single-walled carbon nanotube bundles on flexible plastic substrates," *Journal of the American Chemical Society*, vol. 126, no. 14, pp. 4462–4463, Apr. 2004.

[72] K. Kordás, T. Mustonen, G. Tóth, H. Jantunen, M. Lajunen, C. Soldano, S. Talapatra, S. Kar, R. Vajtai, and P. M. Ajayan, "Inkjet printing of electrically conductive patterns of carbon nanotubes," *Small*, vol. 2, no. 8-9, pp. 1021–1025, Aug. 2006.

[73] T. Kim, H. Song, J. Ha, S. Kim, D. Kim, S. Chung, J. Lee, and Y. Hong, "Inkjet-printed stretchable single-walled carbon nanotube electrodes with excellent mechanical properties," *Applied Physics Letters*, vol. 104, no. 11, Art. no. 113103 (4pp), Mar. 2014.

[74] J. Ding, S. Fu, R. Zhang, E. Boon, W. Lee, F. T. Fisher, and E.-H. Yang, "Graphene—vertically aligned carbon nanotube hybrid on PDMS as stretchable electrodes," *Nanotechnology*, vol. 28, no. 46, Art. no. 465302 (9pp), Nov. 2017.

[75] B. Kumar, H. S. Tan, N. Ramalingam, and S. G. Mhaisalkar, "Integration of ink jet and transfer printing for device fabrication using nanostructured materials," *Carbon*, vol. 47, no. 1, pp. 321–324, Jan. 2009.

[76] E. Song, T. H. da Costa, and J.-W. Choi, "A chemiresistive glucose sensor fabricated by inkjet printing," *Microsystem Technologies*, vol. 23, no. 8, pp. 3505–3511, Aug. 2017.

[77] R. P. Tortorich, E. Song, and J.-W. Choi, "Inkjet-printed carbon nanotube electrodes with low sheet resistance for electrochemical sensor applications," *Journal of The Electrochemical Society*, vol. 161, no. 2, pp. B3044–B3048, 2014.

[78] T. H. da Costa, E. Song, R. P. Tortorich, and J.-W. Choi, "A paper-based electrochemical sensor using inkjet-printed carbon nanotube electrodes," *ECS Journal of Solid State Science and Technology*, vol. 4, no. 10, pp. S3044–S3047, 2015.

[79] C.-X. Liu and J.-W. Choi, "Precision patterning of conductive polymer nanocomposite using a laser-ablated thin film," *Journal of Micromechanics and Microengineering*, vol. 22, no. 4, Art. no. 045014 (8pp), Apr. 2012.

[80] D. J. Guckenberger, T. E. de Groot, A. M. D. Wan, D. J. Beebe, and E. W. K. Young, "Micromilling: a method for ultra-rapid prototyping of plastic microfluidic devices," *Lab on a Chip*, vol. 15, no. 11, pp. 2364–2378, Jun. 2015.

[81] V. Georgakilas, A. Demeslis, E. Ntararas, A. Kouloumpis, K. Dimos, D. Gournis, M. Kocman, M. Otyepka, and R. Zbořil, "Hydrophilic nanotube supported graphene-water dispersible carbon superstructure with excellent conductivity," *Advanced Functional Materials*, vol. 25, no. 10, pp. 1481–1487, Mar. 2015.

[82] M. T. Byrne and Y. K. Gun'ko, "Recent advances in research on carbon nanotube-polymer composites," *Advanced Materials*, vol. 22, no. 15, pp. 1672–1688, Apr. 2010.

[83] R. D. Deegan, O. Bakajin, T. F. Dupont, G. Huber, S. R. Nagel, and T. A. Witten, "Capillary flow as the cause of ring stains from dried liquid drops," *Nature*, vol. 389, pp. 827–829, Oct. 1997.

[84] B. Derby, "Inkjet printing of functional and structural materials: fluid property

requirements, feature stability, and resolution," *Annual Review of Materials Research*, vol. 40, no. 1, pp. 395–414, Jun. 2010.

[85] C. Liu, "Microfabrication of conductive polymer nanocomposite for sensor applications," Ph.D. dissertation, School of Electrical Engineering and Computer Science, Louisiana State University, Baton Rouge, LA, 2012.

[86] K. Lau, M. Lu, H. Cheung, F. Sheng, and H. Li, "Thermal and mechanical properties of single-walled carbon nanotube bundle-reinforced epoxy nanocomposites: the role of solvent for nanotube dispersion," *Composites Science and Technology*, vol. 65, no. 5, pp. 719–725, Apr. 2005.

[87] X. Gong, J. Liu, S. Baskaran, R. D. Voise, and J. S. Young, "Surfactant-assisted processing of carbon nanotube/polymer composites," *Chemistry of Materials*, vol. 12, no. 4, pp. 1049–1052, Apr. 2000.

[88] K. Haubert, T. Drier, and D. Beebe, "PDMS bonding by means of a portable, low-cost corona system," *Lab on a Chip*, vol. 6, no. 12, pp. 1548–1549, 2006.

[89] H.-Z. Geng, K. K. Kim, K. P. So, Y. S. Lee, Y. Chang, and Y. H. Lee, "Effect of acid treatment on carbon nanotube-based flexible transparent conducting films," *Journal of the American Chemical Society*, vol. 129, no. 25, pp. 7758–7759, Jun. 2007.

[90] E. Artukovic, M. Kaempgen, D. S. Hecht, S. Roth, and G. Grüner, "Transparent and flexible carbon nanotube transistors," *Nano Letters*, vol. 5, no. 4, pp. 757–760, Apr. 2005.

[91] F. De Nicola, M. Salvato, C. Cirillo, M. Crivellari, M. Boscardin, M. Scarselli, F. Nanni, I. Cacciotti, M. De Crescenzi, and P. Castrucci, "Record efficiency of air-stable multi-walled carbon nanotube/silicon solar cells," *Carbon*, vol. 101, pp. 226–234, May 2016.

[92] B. DemiRel, A. Yaraş, and H. Elçiçek, "Crystallization behavior of PET materials," *BAÜ Fen Bil. Enst. Dergisi Cilt*, vol. 13, no. 1, pp. 26–35, 2011.

[93] M. Liu, J. Sun, and Q. Chen, "Influences of heating temperature on mechanical properties of polydimethylsiloxane," *Sensors and Actuators A: Physical*, vol. 151, no. 1, pp. 42–45, Apr. 2009.

[94] J. J. Aklonis, W. J. MacKnight, and M. Shen, *Introduction to polymer viscoelasticity*. New York, NY, USA: Wiley-Interscience, 1972.

[95] Y. Ding, E. Huang, K. S. Lam, and T. Pan, "Microfluidic impact printer with interchangeable cartridges for versatile non-contact multiplexed micropatterning," *Lab on a Chip*, vol. 13, no. 10, pp. 1902–1910, May 2013.

[96] Y. Mao, X. Wang, X. Li, B. Li, and J. Chu, "Modelling on the droplet formation and optimizing of the microfluidic cartridge used for the microfluidic impact printing," *Journal of Micromechanics and Microengineering*, vol. 29, no. 12, Art. no. 125016 (10pp), Dec. 2019.

[97] J.-U. Park, M. Hardy, S. J. Kang, K. Barton, K. Adair, D. kishore Mukhopadhyay, C. Y. Lee, M. S. Strano, A. G. Alleyne, J. G. Georgiadis, P. M. Ferreira, and J. A. Rogers, "High-resolution electrohydrodynamic jet printing," *Nature Materials*, vol. 6, no. 10, pp. 782–789, Oct. 2007.

[98] Hewlett-Packard Company, "HP extended TIJ 1.0 print cartridges," HP® Official Site. https://www8.hp.com (accessed: Nov. 07, 2019).

[99] J.-W. Song, J. Kim, Y.-H. Yoon, B.-S. Choi, J.-H. Kim, and C.-S. Han, "Inkjet printing of single-walled carbon nanotubes and electrical characterization of the line pattern," *Nanotechnology*, vol. 19, no. 9, Art. no. 095702 (6pp), Mar. 2008.

[100] T. Wang, M. A. Roberts, I. A. Kinloch, and B. Derby, "Inkjet printed carbon nanotube networks: the influence of drop spacing and drying on electrical properties," *Journal of Physics D: Applied Physics*, vol. 45, no. 31, Art. no. 315304 (8pp), Aug. 2012.

[101] S. Azoubel, S. Shemesh, and S. Magdassi, "Flexible electroluminescent device with inkjet-printed carbon nanotube electrodes," *Nanotechnology*, vol. 23, no. 34, Art. no. 344003 (6pp), Aug. 2012.

[102] B. S. Cook and A. Shamim, "Inkjet printing of novel wideband and high gain antennas on low-cost paper substrate," *IEEE Transactions on Antennas and Propagation*, vol. 60, no. 9, pp. 4148–4156, Sep. 2012.

[103] W. C. Oliver and G. M. Pharr, "An improved technique for determining hardness and elastic modulus using load and displacement sensing indentation experiments," *Journal of Materials Research*, vol. 7, no. 06, pp. 1564–1583, Jun. 1992.

[104] C.-X. Liu and J.-W. Choi, "Analyzing resistance response of embedded PDMS and carbon nanotubes composite under tensile strain," *Microelectronic Engineering*, vol. 117, pp. 1–7, Apr. 2014.

[105] C.-X. Liu and J.-W. Choi, "Strain-dependent resistance of PDMS and carbon nanotubes composite microstructures," *IEEE Transactions on Nanotechnology*, vol. 9, no. 5, pp. 590–595, Sep. 2010.

[106] L. Yu, B. Kim, and E. Meng, "Chronically implanted pressure sensors: challenges and state of the field," *Sensors*, vol. 14, no. 11, pp. 20620–20644, Nov. 2014.

[107] D. L. Grieco, L. Chen, and L. Brochard, "Transpulmonary pressure: importance and limits," *Annals of Translational Medicine*, vol. 5, no. 14, pp. 285–285, Jul. 2017.

[108] N. Ida, "Mechanical sensors and actuators," in *Sensors, Actuators, and Their Interfaces - A Multidisciplinary Introduction*, Edison, NJ, USA: SciTech, 2014, pp. 281–334.

[109] S. Beeby, G. Ensell, M. Kraft, and N. White, *MEMS mechanical sensors*. Norwood, MA, USA: Artech House, 2004.

[110] H.-P. Loock and P. D. Wentzell, “Detection limits of chemical sensors: applications and misapplications,” *Sensors and Actuators B: Chemical*, vol. 173, pp. 157–163, Oct. 2012.

[111] T. Xu, H. Wang, Y. Xia, Z. Zhao, M. Huang, J. Wang, L. Zhao, Y. Zhao, and Z. Jiang, “Piezoresistive pressure sensor with high sensitivity for medical application using peninsula-island structure,” *Frontiers of Mechanical Engineering*, vol. 12, no. 4, pp. 546–553, Dec. 2017.

[112] A. S. Fiorillo, C. D. Critello, and S. A. Pullano, “Theory, technology and applications of piezoresistive sensors: a review,” *Sensors and Actuators A: Physical*, vol. 281, pp. 156–175, Oct. 2018.

[113] R. Helgason, A. Campigotto, and Y. Lai, “The development of a pressure sensor using a technique for patterning silver nanowires on 3-dimensional curved PDMS membranes,” *Journal of Micromechanics and Microengineering*, vol. 30, no. 9, Art. no. 095013 (12pp), Sep. 2020.

[114] M. Chovancová and J. Elcner, “The pressure gradient in the human respiratory tract,” *EPJ Web of Conferences*, vol. 67, Art. no. 02047 (6pp), 2014.

[115] I. Ayappa and D. M. Rapoport, “The upper airway in sleep: physiology of the pharynx,” *Sleep Medicine Reviews*, vol. 7, no. 1, pp. 9–33, Feb. 2003.

[116] G. Yuan, N. A. Drost, and R. A. McIvor, “Respiratory rate and breathing pattern,” *McMaster University Medical Journal*, vol. 10, no. 1, pp. 23–25, 2013.

[117] P. Vock, T. Spiegel, E. K. Fram, and E. L. Effmann, “CT assessment of the adult intrathoracic cross section of the trachea,” *Journal of Computer Assisted Tomography*, vol. 8, no. 6, pp. 1076–1082, Dec. 1984.

[118] G. Doucet, S. Ryan, M. Bartellas, M. Parsons, A. Dubrowski, and T. Renouf, “Modelling and manufacturing of a 3D printed trachea for cricothyroidotomy simulation,” *Cureus*, vol. 9, no. 8, Art. no. e1575 (14pp), Aug. 2017.

[119] L. L. Gingrich, “Relation among age, gender, and oral/palatal dimensions on anterior and posterior lingual-palatal pressures in healthy adults,” Ph.D. dissertation, Florida State University, Tallahassee, FL, 2011.

VITA

Tallis Huther da Costa was born in Humaita, RS, Brazil. He received his B.E. degree in Computer Engineering from Pontifical Catholic University of Rio Grande do Sul, Brazil, in 2013. He joined Louisiana State University in 2013 for the doctoral program in Electrical Engineering. His research is on fabrication methods for flexible sensors.

List of Author's Publications

Journal Papers

1. **T. H. da Costa** and J.-W. Choi, "Fabrication and patterning methods of flexible sensors using carbon nanomaterials on polymers," Advanced Intelligent Systems, vol. 2, article 1900179, 2020.

2. **T. H. da Costa** and J.-W. Choi, "Low-cost and customizable inkjet printing for microelectrodes fabrication," Micro and Nano Systems Letters, vol. 8, article 2, 2020.

3. P. J. Chacon, L. Pu, **T. H. da Costa**, Y.-H. Shin, T. Ghomian, H. Shamkhalichenar, H.-C. Wu, B. A. Irving, and J.-W. Choi, "A wearable pulse oximeter with wireless communication and motion artifact tailoring for continuous use," IEEE Trans Biomed Eng, vol. 66, pp. 1505–1513, 2019.

4. **T. H. da Costa** and J.-W. Choi, "A flexible two dimensional force sensor using PDMS nanocomposite," Microelectronic Engineering, vol. 174, pp. 64–69, 2017.

5. E. Song, **T. H. da Costa**, and J.-W. Choi, "A chemiresistive glucose sensor fabricated by inkjet printing," Microsystem Technologies, vol. 23, issue 8, pp. 3505-3511, 2016.

6. **T. H. da Costa**, E. Song, R. P. Tortorich, and J.-W. Choi, "A paper-based electrochemical sensor using inkjet-printed carbon nanotube electrodes," ECS Journal of Solid State Science and Technology, vol. 4, no. 10, pp. S3044–S3047, 2015.

7. E. Song, R. P. Tortorich, **T. H. da Costa**, and J.-W. Choi, "Inkjet printing of conductive polymer nanowire network on flexible substrates and its application in chemical sensing,"

Microelectronic Engineering, vol. 145, pp. 143–148, 2015.

Conference Manuscripts

1. Y. Xie, Y.-C. Lee, **T. H. da Costa**, J. Park, J. H. Jui, J.-W. Choi, and Z. Zhang, "Construction data-driven dynamic sound data training and hardware requirements for autonomous audio-based site monitoring," in Proceedings of the 36th International Symposium on Automatic and Robotics in Construction (ISARC 2019), Banff, AB, Canada, May 21-24, pp. 1011-1017, 2019.
2. R. P. Tortorich, **T. H. da Costa**, E. Song, and J.-W. Choi, "A printed carbon nanotube sensor on a flexible substrate," ECS Transactions, vol. 64, issue 1, pp. 175-179, 2014.

Conference Abstracts

1. T. H. da Costa and J.-W. Choi, "A highly sensitive pressure sensor based on carbon nanotubes and polymer composite," The 45th International Conference on Micro Nano Engineering (MNE 2019), Rhodes, Greece, September 23-26, 2019.
2. J.-W. Choi, T. H. da Costa, J. Seo, J.-W. Kim, and S. J. Kim, "A polymer pressure sensor for sleep apnea monitoring," The 30th Conference of the Society for Medical Innovation and Technology (SMIT 2018) and International Biomedical Engineering Conference (IBEC 2018), Seoul, Korea, November 8-10, 2018.
3. T. H. da Costa, J. Seo, S. J. Kim, J.-W. Kim, and J.-W. Choi, "Breathing detection using a polymer pressure sensor," International Symposium on Information Technology Convergence 2018 (ISITC 2018), Jeonju, Korea, October 24-27, 2018.
4. J. A. P. Amaya, T. H. da Costa, R. Koh, and J.-W. Choi, "Wearable smartphone-controlled stimulator system for veterinary electro-acupuncture," 2018 BMES Annual Meeting, October 17-20, 2018, Atlanta, Georgia.
5. T. H. da Costa and J.-W. Choi, "Detection of underwater pressure vibrations with an elastomer-based sensor," The 44th International Conference on Micro Nano Engineering (MNE 2018), Copenhagen, Denmark, September 24-27, 2018.
6. T. H. da Costa and J.-W. Choi, "An all elastomer pressure sensor utilizing printed carbon nanotube patterns," The 43rd International Conference on Micro Nano Engineering (MNE 2017), Braga, Portugal, September 18-22, 2017.
7. T. H. da Costa and J.-W. Choi, "A printed capacitor with carbon nanotube electrodes for energy storage," The 231st Electrochemical Society Meeting, New Orleans, LA, May 28 – June 1, 2017.
8. T. H. da Costa and J.-W. Choi, "A flexible two dimensional force sensor using PDMS nanocomposite," The 42nd International Conference on Micro and Nano Engineering (MNE 2016), Vienna, Austria, September 19-23, 2016.

9. P. J. Chacon, Y.-H. Shin, T. Ghomian, H. Shamkhalichenar, T. H. da Costa, and J.-W. Choi, “Wearable reflectance-type pulse oximeter design with wireless communication capability for blood oxygenation monitoring,” The 38th Annual International Conference of the IEEE Engineering in Medicine and Biology Society (IEEE EMBC 2016), Orlando, FL, August 16-20, 2016.

10. T. H. da Costa and J.-W. Choi, “A flexible two dimensional force sensor using PDMS nanocomposite,” US-Korean Conference on Science, Technology, and Entrepreneurship 2016 (UKC 2016), Dallas, TX, August 10-13, 2016.

11. T. H. da Costa and J.-W. Choi, “A dopamine sensor on paper with printed carbon nanotube electrodes,” The 41st International Conference on Micro and Nano Engineering (MNE 2015), The Hague, Netherlands, September 21-24, 2015.

12. T. H. da Costa, R. P. Tortorich, E. Song, and J.-W. Choi, "A fully inkjet-printed carbon nanotube electrochemical sensor on paper," 227th Electrochemical Society Meeting, Chicago, IL, May 2015

13. T. H. da Costa and J.-W. Choi, “A flexible force sensor using printed carbon nanotubes on PDMS by transfer patterning,” The 40th International Conference on Micro and Nano Engineering (MNE 2014), Lausanne, Switzerland, September 22-26, 2014.